Technischen Universität München

Fakultät für Medizin

The evaluation of intraoperative MRI-based elastic fusion for brain shift compensation of preoperative DTI tractography

Wei Zhang

Vollständiger Abdruck der von der Fakultät für Medizin der TechnischenUniversität München zur Erlangung des akademischen Grades eines

Doktors der Medizin (Dr. med.)

genehmigten Dissertation.

Vorsitz: apl. Prof. Dr. Bernhard Haslinger

Prüfende/-r der Dissertation:

1. apl. Prof. Dr. Sandro M. Krieg
2. Priv.-Doz. Dr. Valentin Riedl, Ph.D.

Die Dissertation wurde am 21.06.2022 bei der Technischen Universität München eingereicht und durch die Fakultät für Medizin am 08.11.2022 angenommen.

The portion of contents presented in this dissertation was modified from an original article which has been published with the following title:

Wei Zhang, Sebastian Ille, Maximilian Schwendner, Benedikt Wiestler, Bernhard Meyer, Sandro M. Krieg. Tracking motor and language eloquent white matter pathways with intraoperative fiber tracking versus preoperative tractography adjusted by intraoperative MRI-based elastic fusion. J Neurosurg. Feb 25 2022:1-10. doi:10.3171/2021.12.JNS212106 (Zhang et al., 2022).

TABLE OF CONTENTS

ABBREVIATIONS

3D:	three-dimensional
AF:	arcuate fasciculus
ASD:	average surface distance
BA	Brodmann area
CT:	computerized tomography
CSF:	cerebrospinal fluid
CST:	corticospinal tract
DES:	direct electrical stimulation
DICE:	dice coefficient
DTI:	diffusor tensor imaging
EF:	elastic fusion
EOR:	extent of resection
EPI	echo planar imaging
FA:	fractional anisotropy
FACT:	fiber assignment by continuous tracking
FAT:	fractional anisotropy threshold
FEM:	finite element modeling
fMRI:	functional magnetic resonance imaging
FT:	fiber tracking
GTR:	gross total resection
GO:	group of operated hemispheres

GNO:	group of non-operated hemispheres
HD:	Hausdorff distance
HGG:	high-grade glioma
IBEF:	intraoperative magnetic resonance imaging-based elastic fusion
IGNS:	image-guided neuronavigation systems
ioCT:	intraoperative computerized tomography
ioLRS:	intraoperative laser range scan
ioMRI:	intraoperative magnetic resonance imaging
ioUS:	intraoperative ultrasounds
IQR:	interquartile range
LGG:	low-grade glioma
MEG:	Magnetoencephalography
MFL:	minimum fiber length
nTMS:	navigated Transcranial Magnetic Stimulation
PET:	positron emission tomography
pMRI:	preoperative magnetic resonance imaging
RF:	rigid fusion
ROI:	region of interest

1. INTRODUCTION

1.1 Image-Guided Neurosurgical Systems

Neurosurgery involves the surgical intervention of the brain that requires exact orientation. Improved accuracy due to intraoperative neuronavigation technology greatly reduced the incidence of complications. Three-dimensional (3D) presentation of intraoperative brain structures and stereoscopic navigation gives neurosurgeons a direct visualization instead of reconstructing the spatial relationship of tumor and other critical brain structures only based on years of experience and the ability of spatial imagination.

Image-guided neuronavigation systems (IGNS) are widely used in modern neurosurgical practice, aid neurosurgeons in planning operations preoperatively, and supply orientation and localization intraoperatively (Thomas & Sinclair, 2015). In the last few decades, image-guided neurosurgical technology has been developed and has demonstrated a large advantage with a higher level of precision compared to conventional preoperative neurosurgery planning, which requires reconstructing the size and location of the lesion in the neurosurgeon's mind based on viewing the preoperative image and relevant anatomic landmarks (Enchev, 2009; Wadley et al., 1999a; Wadley et al., 1999b). In 1986, Roberts et al. developed and described the first frameless and interactive image-guide system by acoustic tracking and computerized tomography (CT) imaging (Roberts et al., 1986). Bucholz and McDurmont later integrated various technologies, including optical tracking, skull-based reference frames, and computer visualization and monitoring, into one system in the 1990s (Bucholz & McDurmont, 2009). This combined system was technically upgraded and became StealthStation (Medtronic Navigation, Louisville, CO, USA), which was acquired and commercially marketed by Medtronic in 1999 (Azagury et al., 2015; Bucholz & McDurmont, 2009). StealthStation, previously known as Neurostation, is considered the first image guidance system consisting of all fundamental elements of contemporary IGNS (Azagury et al., 2015; Bucholz & McDurmont, 2009).

Specifically, modern IGNS can transform the physical space coordinates established by skull-based reference system to the coordinates of selected preoperative images first. This important process is known as registration. Next, the position of the surgical probe is detected by an optical tracking camera. The position of anatomical structure is ultimately displayed on the monitoring screen in real-time (Figure 1). To do so, 3D images with high resolution are required. Apart from 3D CT, magnetic resonance imaging (MRI) is commonly utilized for pre-neurosurgical planning (Azagury et al., 2015; Enchev, 2009; Ivanov & Ciurea, 2009; Thomas & Sinclair, 2015). Preoperative magnetic resonance imaging (pMRI) is standardly used for image-guided neuronavigation and surgical planning in brain tumor resection, and also shows higher accuracy and safety compared to conventional brain tumor localization (Mahvash et al., 2017; Prada et al., 2015).

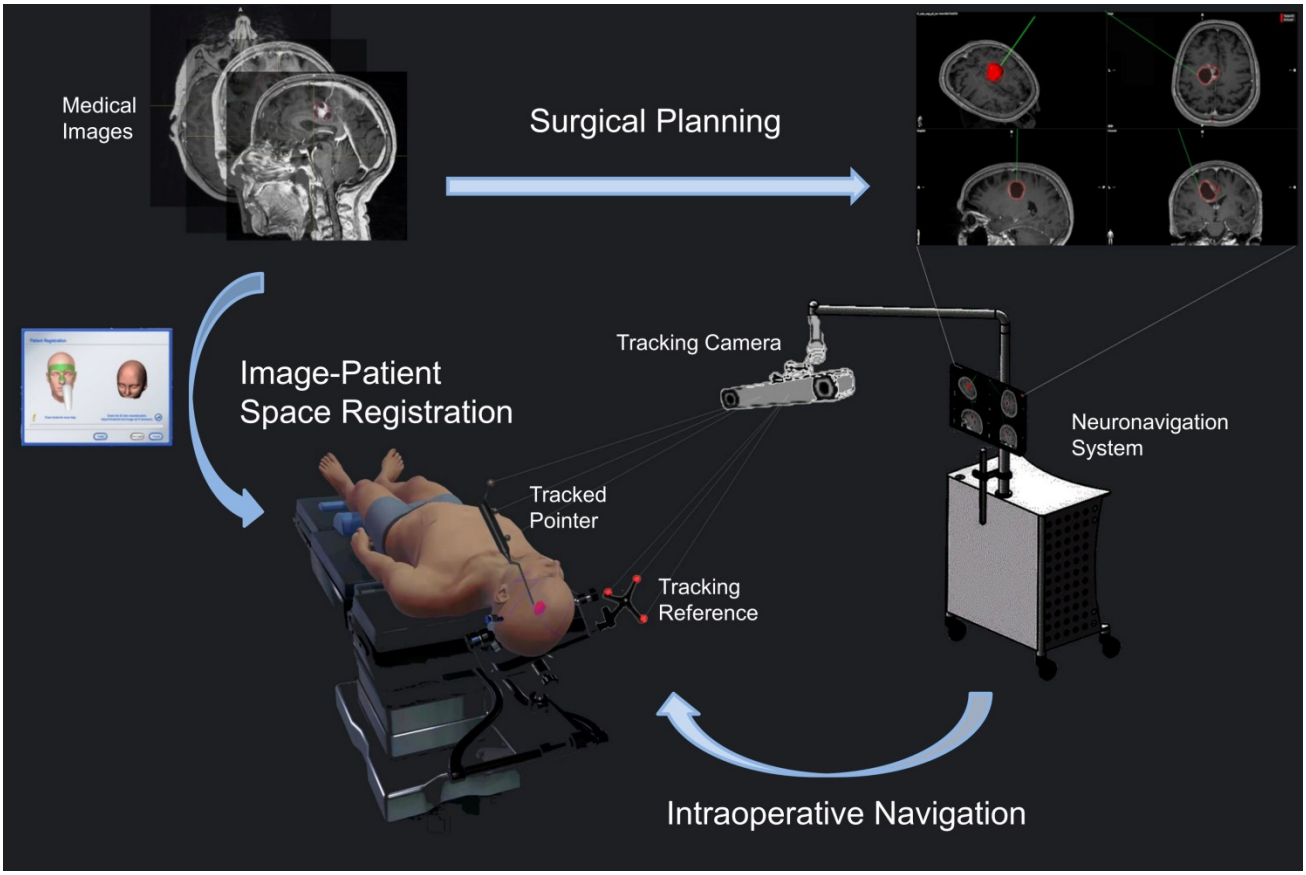

Figure 1: The diagram of image-guided neuronavigation systems

Image-guided neuronavigation system contains an optical tracking camera, a tracking reference attached to head fixation device, a computer workstation with navigation software that can register patient's

physical space on 3D medical images through the face or skull landmarks and visualize the space relationship, a monitoring screen which can display the position of tracked pointer to guide surgeons intraoperatively.

1.2 Functional Brain Imaging in IGNS

Apart from structural imaging, functional imaging can also be added into IGNS to provide neurosurgeons with more information for preoperative surgical planning and intraoperative guidance (Brahimaj et al., 2021; Tharin & Golby, 2007). Especially when considering functional reorganization of the motor cortex and the language network induced by brain tumors, the necessity of preoperatively functional mapping and subsequent reconstruction of corresponding fiber tractography becomes evident (Baciu et al., 2003; Barz et al., 2018; Ille et al., 2019; Lubrano et al., 2010). This individual functional mapping combined with IGNS and intraoperative monitoring can then reduce the rates of surgery-related deficits (Ottenhausen et al., 2015). Several types of functional brain imaging can be integrated into IGNS to identify the eloquent brain area efficiently and accurately. Functional magnetic resonance imaging (fMRI) fused with anatomical images can demonstrate the functional area in neuronavigation system to preoperatively evaluate the risks and safely resect the lesion (Roux et al., 1997; Sabbah et al., 2000). Furthermore, the integration of fMRI and positron emission tomography (PET) into neuronavigation can visualize the active brain areas while distinguishing them from tumor and edema (Braun et al., 2000). Moreover, functional areas located by Magnetoencephalography (MEG) can be superimposed onto anatomical images and then in combination be imported into neuronavigation systems (Ganslandt et al., 1999; Stufflebeam, 2011). As the newest addition, navigated Transcranial Magnetic Stimulation (nTMS) is employed as a novel non-invasive method to detect functional brain areas (Krieg et al., 2017; Sollmann et al., 2018a; Sollmann et al., 2021).

Compared to the various functional imaging techniques on cortical level mentioned above, diffusion

MRI is a unique non-invasive technology to display vivo white matter tracts on subcortical level (Leclercq et al., 2011). Fiber tracking (FT) based on diffusion tensor imaging (DTI) can be utilized to display selected white matter pathways around the lesion in IGNS and, therefore, plays a major role in neurosurgical planning (Alexopoulos et al., 2019; Dubey et al., 2018). The integration of DTI FT into neuronavigation system has been proven reliable and provides crucial data of the localization of fiber tracts and their relationship to lesions (Nimsky et al., 2007) (Figure 2). DTI FT based on cortical functional imaging can demonstrate functional neural pathways on structural images in three dimensions and guide neurosurgeons to achieve maximized resection of brain lesions while maximizing the protection of brain function intraoperatively (Kamada et al., 2003; Sollmann et al., 2016; Sollmann et al., 2018b). In addition to intraoperative mapping, IGNS combined with cortical or subcortical direct electrical stimulation (DES) is regarded as the golden standard for locating the eloquent cortex or fibers in clinical practice, although the physiological effects of the method are not completely understood (Borchers et al., 2011; Munnich et al., 2019). DES is an invasive procedure that stimulates the cortical surface or the margin of the resection cavity with an electrode. The positive points are detected when transitory behavioral changes of motor, language and cognition can be produced repeatedly (Borchers et al., 2011). Awake craniotomy technique combined with DES is a widely used method to identify functional hotspots during the operation (Chua et al., 2018; Hervey-Jumper et al., 2015). Previous studies indicate a good concordance between DTI FT and DES with a high level of sensitivity and specificity both in terms of motor and language function (Bello et al., 2008; Leclercq et al., 2010).

Hence, through using neuronavigation based on functional brain imaging and DTI FT, functionally active areas and connected networks can be detected in relation to infiltrative brain tumors, providing more information to support clinical decision making (Daniel et al., 2021; Ganslandt et al., 2004; Roux et al., 1997; Schiffbauer et al., 2001).

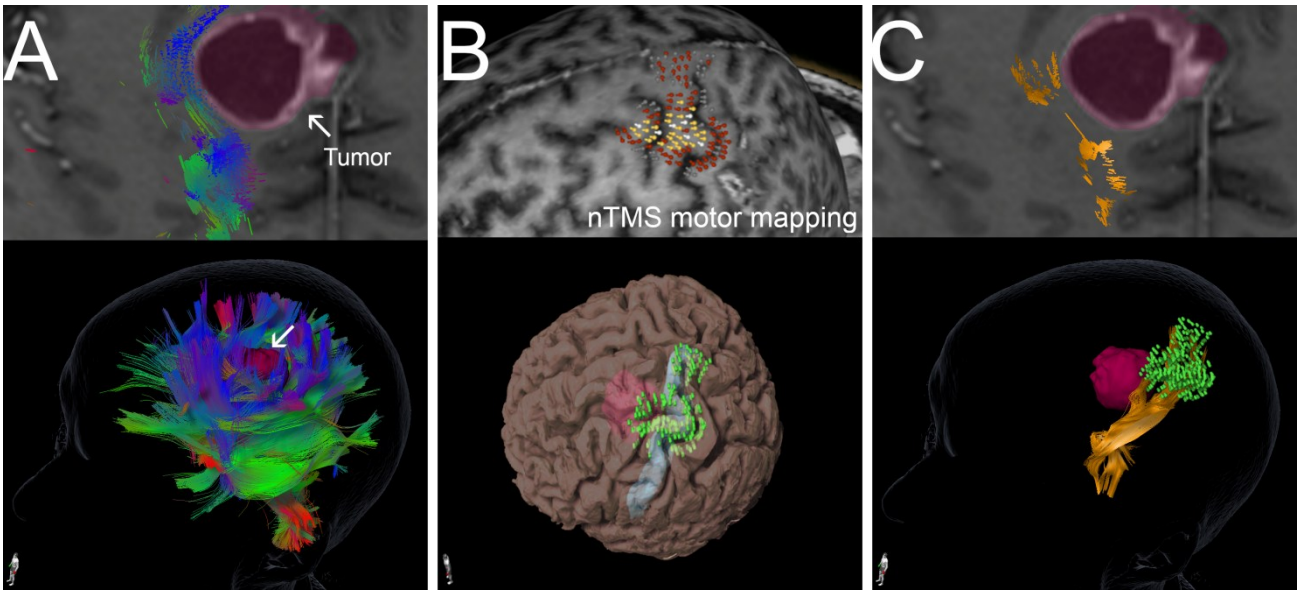

Figure 2: nTMS motor mapping combines with DTI FT to display functional white matter pathways

Diffusion tensor imaging (DTI)-based fiber tracking (FT) can provide information of white matter pathways (Figure A). However, without functional mapping, the FT is unselected and bewildering. Navigated Transcranial Magnetic Stimulation (nTMS) motor mapping (Figure B) combined with DTI FT can provide selected functional white matter pathways and display their relationship to the lesion in 3D space (Figure C).

1.3 Brain Shift

The major objective of neuronavigation is to minimize the errors of target localization intraoperatively. However, numerous factors impact the accuracy of neuronavigation systems leading to spatial errors between physical locations of brain tissue and virtual points of preoperatively registered images (Gerard et al., 2017). Various physical factors can cause the displacement of the spatial position of the IGNS reference frame, including the attachment of surgical drapes, skin retractors and brain tissue retractor systems, the utilization of surgical instruments such as drills and craniotomes during craniotomy, and the relative displacement between the patient's head and the head holder, which progressively increases over surgery time (Stieglitz et al., 2013; Wang & Song, 2011). Technical factors that induce deviation are caused by technical limitations of IGNS, including inhomogeneous

reflection of infrared light flashes, errors of patient-image co-registration, and the limited resolution of medical images (Gerard & Collins, 2015; Stieglitz et al., 2013; Wang & Song, 2011). Brain shift is the biggest biological factor impacting the accuracy of IGNS during the entire operation procedure (Thomas & Sinclair, 2015). The procedure of neurosurgical operation can be more efficient after the compensation of brain shift (Nimsky et al., 2001).

In 1986, Kelly et al. first reported the phenomenon of brain shift (Kelly et al., 1986). Since then, various reasons for this phenomenon have been described (Gerard et al., 2017): As the main factor contributing to brain shift, the effects of gravity have been identified as it leads to sagging of the tissue and the loss of cerebrospinal fluid (CSF) after the dura opening (Nabavi et al., 2001). In general, brain shift is unpredictable whenever the brain tissue around the resection cavity loses support and collapses (Hastreiter et al., 2004; Nabavi et al., 2001). Moreover, changes in pressure of the intracranial cavity arising from CSF loss and intracranial air emergence during neurosurgery can further aggravate brain shift (Coenen et al., 2011; Elias et al., 2007). Other effects include different head positioning between images acquisition preoperatively and surgical procedure intraoperatively before the dura opening (Stieglitz et al., 2013; Yokoyama et al., 2021). The utilization of Mannitol to reduce intracranial pressure can also result in increased brain shift (Benveniste & Germano, 2005; Li et al., 2020). For those mentioned reasons, subcortical brain regions on different levels can intraoperatively shift in various directions and distances, leading to an increased risk of surgery-related deficits (Khalid et al., 2017; Nimsky et al., 2005). Since precision in location-relevant anatomical targets is notably crucial for neurosurgical intervention, brain shift needs to be corrected as damage to nearby structures can lead to unexpected injuries and unnecessary surgery-related neurological deficits during the operation (Figure 3).

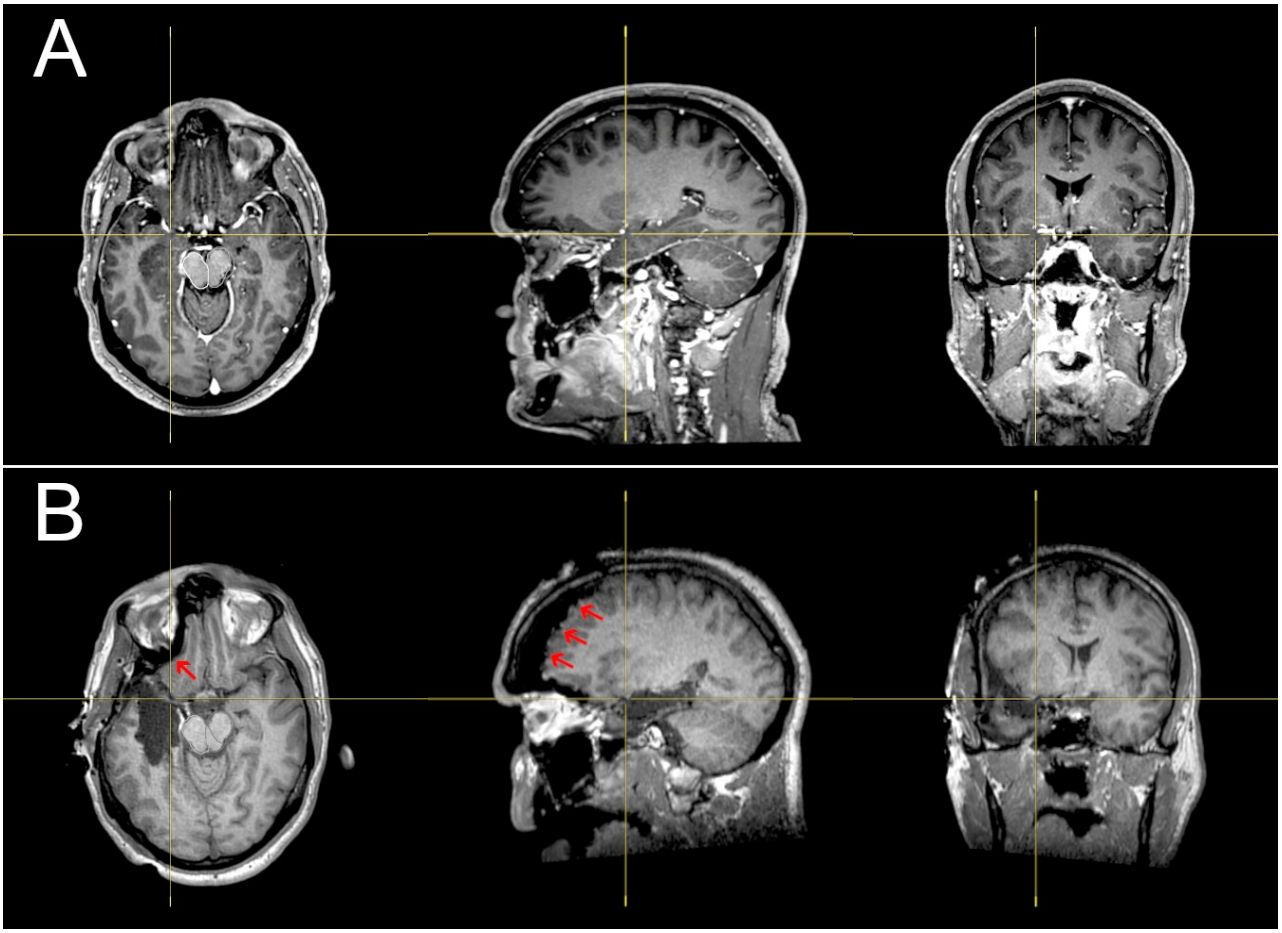

Figure 3: Example of brain shift in real case

An example of brain shift in clinical case which performed left temporal lobe tumor resection. When compared to preoperative images (Figure A), intraoperative images (Figure B) show that the left frontal lobe has an obvious location shift (red arrows), and the whole brain tissue is compressed backward after operation.

1.4 Compensation Methods of Brain Shift: Benefits and Drawbacks

To compensate for brain shift, three basic methods and their combinations have been summarized and reported previously: registration of intraoperative image, predictive modeling, and biomechanical modeling (Gerard et al., 2017). Yet, the best method still has not been determined as these compensation methods so far have remarkable advantages and obvious shortages.

1.4.1 Registration of intraoperative image

Many approaches can be used for intraoperative image acquisition and can be registered to IGNS and update the target location. The list includes intraoperative MRI (ioMRI) and CT (ioCT), ultrasounds (ioUS) and other local stereo image acquisition tools including laser range scan (ioLRS) and stereo camera (Cao et al., 2008; Kuhnt et al., 2012; Mahboob et al., 2016; Schichor et al., 2017; Sinha et al., 2005). Updating of the intraoperative image can be intraoperatively performed one to several times, or even in a continuous fashion implementing real-time updates.

Registration of ioMRI is one of the options to adjust the accuracy of neuronavigation. It is considered the most reliable method of compensating for brain shift, providing a more precise neuronavigation (Bayer et al., 2017; Nimsky et al., 2001). However, the disadvantages of ioMRI, including the prolonged operation time and the additional costs, have to be taken into account. The method of ioCT, which consist of intraoperative CT angiography for vessel structure as well, is also a common way to update the navigation system but entails the risk of ionizing radiation exposure to patients and surgery team (Carl et al., 2018; Schichor et al., 2017). Lastly, ioUS and ioLRS can be used as a real-time update method for superficial anatomical targets, but these techniques are characterized by a sole focus on local tissue region and cannot acquire the whole brain images (Prada et al., 2015; Sinha et al., 2005).

To update functional images, intraoperative DTI FT is regarded to be a viable method for visualizing fiber tracts precisely (Javadi et al., 2017; Maesawa et al., 2010; Ostry et al., 2013). Fiber tracts can be reconstructed by a combination of intraoperative diffusion-tensor tractography with intraoperative DES mapping and neurophysiological monitoring during awake neurosurgery (Bello et al., 2008; Maesawa et al., 2010; Munnich et al., 2019). Intraoperative functional ultrasound can also be used for cortical mapping by detecting changes in blood volume during task-evoked cortical responses when the patient is awakened (Imbault et al., 2017). However, the full cooperation of the patient

during awake neurosurgery is necessary, as well as higher requirements of the operation team for anesthesia techniques and the high degree of collaboration between neurosurgeons and anesthesiologists. Furthermore, the additional acquisition of intraoperative diffusion imaging is often restricted and questioned in clinical practice, mainly due to technical limitations of the scanner, quality factors, and lengthy setup time (Kuhnt et al., 2012; Nimsky, 2011). Besides, analyzable intraoperative DTI data likely fail to be acquired, or be disturbed significantly by various artifacts, as intraoperative DTI data often is of low quality due to the impact of air-brain interface, edemas in the vicinity of the resection, as well as the complicated signal in the areas of resection cavity and tumor remnants (Maesawa et al., 2010; Nimsky, 2011). As a result, the existing fibers are not tracked and visualized correctly. When intraoperative functional data cannot be achieved for various reasons and preoperative functional images become the only reference source, the approach of fusing preoperative functional images with intraoperative structural images is an alternative measure as a solution for these disadvantages. During tumor resection, however, images are commonly co-registered rigidly with no brain shift compensation. This approach, which is often defined as rigid fusion (RF), was shown to be imprecise in a number of prior researches (Kuhnt et al., 2012; Munnich et al., 2019; Nimsky et al., 2006; Romano et al., 2011).

1.4.2 Predictive modeling with limited deformation data

When complete deformation data of the whole brain cannot be acquired intraoperatively, an available approach was developed, which uses sparse brain shift data and biomechanical modeling to compute and predict the deformation of surface brain tissue, deep structure or even the entire brain (Dumpuri et al., 2007; Morin et al., 2017; Skrinjar et al., 2002; Yu et al., 2022; Zhuang et al., 2011).

As ioUS and ioLRS can acquire surface or subsurface image data from exposed parts of brain intraoperatively with a great capability of real-time update, the predictive models based on these sparse data have the ability to simulate the behavior of brain shift and to predict the deformation of

adjacent brain tissue (Morin et al., 2017; Zhuang et al., 2011). The brain surface information can be acquired by either a set of intraoperative navigated physical surface points that are manually placed and recorded, or by reconstruction of the exposed brain surface with a stereo camera (Skrinjar et al., 2002). Hence, these models are suitable for operations on superficial parts of the brain, or neurosurgical interventions that concern small deformations. Moreover, predictive modeling should be used with caution for functional navigation if the lesion is found in or around functional areas. It has clear limitations when deformations of deep tissue and complex structures need to be attended to.

Pure predictive mathematical models, which are only based on atlas data and pre-computed characteristics of brain shift derived from gravity and CSF drainage, can also be utilized to correct preoperative images (Dumpuri et al., 2007). Predictive modeling demonstrated its ability in the prediction of surface and subsurface shifts when lesion resection and intraoperative traction were not considered (Dumpuri et al., 2010). However, up to the date, the prediction of deep tissue deformation using several simulation drives and considering the impact of gravity, corticospinal fluid loss, boundary conditions and tumor resection, remains to be improved and verified (Yu et al., 2022).

1.4.3 Biomechanical modeling combined with intraoperative images

From a technical point of view, intraoperative imaging-based biomechanical modeling has extensive crossover with predictive modeling. The main difference between the present model and predictive modeling is that, instead of sparse brain shift data, intraoperative images with complete volumetric data of brain deformation increase the accuracy of the biomechanical model-based simulation. The general procedure of brain shift compensation based on biomechanical model and intraoperative images is to process preoperative images by modeling firstly, and then to deform the modeled image based on the intraoperative images which have complete structural brain data (Bayer et al., 2017). To achieve this, ioMRI or ioCT are usually acquired.

Several biomechanical models, which are based on either linear elastic modeling or nonlinear elastic modeling, have been illustrated in a previous review (Gerard et al., 2017). Linear elastic modeling focuses on the stress-strain deformation between stiff tissue and soft tissue, while nonlinear elastic modeling focuses on deformation among soft tissues. The aforementioned two models combined with viscoelastic modeling and biphasic modeling were referred to as constitutive model by Bayer et al. (Bayer et al., 2017). Hereinto, viscoelastic modeling entails the addition of time-depended strain rate, while biphasic modeling regards the brain tissue as a composition of soft tissue and fluid. Finite element analysis, also named finite element modeling (FEM), is a frequently used basic analytical method in numerous approaches of modern 3D biomechanical modeling (Bayer et al., 2017; Dumpuri et al., 2007; Ferrant et al., 2001; Morin et al., 2017; Riva et al., 2019; Skrinjar et al., 2002; Yu et al., 2022; Zhuang et al., 2011). FEM computes patient-specific volumetric brain data, which is segmented into multiple connected mesh 3D elements. According to the shape of the elements, FEM can be categorized as tetrahedral elements, pentahedral elements, or hexahedral elements. The more faces the mesh element has, the less flexibility it has, but in turn it computes the analysis faster (Bayer et al., 2017). Several pre-computed drives which are commonly used in predictive modeling are also applied in intraoperative imaging-based biomechanical model frameworks to simulate brain shift behaviors (Ferrant et al., 2001).

1.5 Model-based Elastic Fusion on Multi-modal Images

In clinical practice, preoperative imaging including anatomical and functional images is abundantly performed to acquire as much information about the target lesion as possible. However, due to intraoperative time constraints and technical limitations, not all modals of preoperative images can be updated by reimaging to completely compensate for brain shift. The model-driven algorithms based on intraoperative images also need to seek a balance between precision and speed to conform to the actual scenario of neurosurgical surgery.

In consideration of these problems, Brainlab AG developed and commercialized a novel tool of elastic fusion (EF) to compensate for brain shift in a time-saving manner. The approach enables to elastically fuse the preoperative multi-model images in IGNS in real clinical practice (Virtual iMRI Cranial, Brainlab Elements®, Brainlab AG, Munich, Germany). The algorithm of elastic fusion was described in several previous articles (Ille et al., 2021a; Negwer et al., 2020; Riva et al., 2019). The process of EF can be divided into three main steps (Figures 4 and 5):

1. Image segmentation of individual preoperative images is calculated based on an atlas model (Synthetic Tissue Model). The multi-modal dataset of different anatomical and functional MRI images, such as T1- and T2-weighted images, FLAIR, DWI, and DTI tractography, can be fused and implemented in the segmentation process simultaneously. This patient-specific model is built to distinguish and label stiff tissues (skull, cerebral falx and the tentorium) and soft tissues.

2. A FEM-based biomechanical model with 1 cm^3 hexahedral mesh elements is then performed to calculate collisions and deformations on segmented preoperative images. Linear elasticity with a co-rotational correction is applied while resolving material properties at subelement level to calculate and correct the stress-strain relationship between the elements of stiff and soft tissue. Several physical forces are considered in terms of load and boundary conditions, such as soft tissues collapsing caused by gravity and hydrostatic pressure, which could be obtained from intraoperative image data. The collisions of adjacent sulci are also considered and computed to simulate specific behaviors of brain shift during this EF calculation.

3. A multi-rigid fusion with 3 x 3 x 3 cm^3 moving units between the simulated preoperative MRIs and intraoperative anatomical images, derived from either ioMRI or ioCT, is applied to roughly match the images. Mutual information metric is used to maximize the local similarity of both simulated preoperative images and native intraoperative images. The deformation field of brain is compensated by interpolation of local fusion estimates and then transferred to the simulated

preoperative MRIs. The volume of resection cavity needs to be user-defined manually to be excluded from the fusion process.

Hereby, a set of deformed preoperative multi-modal MR images can be outputted and displayed in IGNS. Hence, after implementation of the aforementioned steps, intraoperative image-based EF (IBEF) is able to compensate for the brain displacement occurring after the dura opening and tumor resection. Thus, IBEF calculates the deformation of preoperative anatomical images based on intraoperative anatomical images. The computation of compensation is theoretically able to be converted to preoperative tractography.

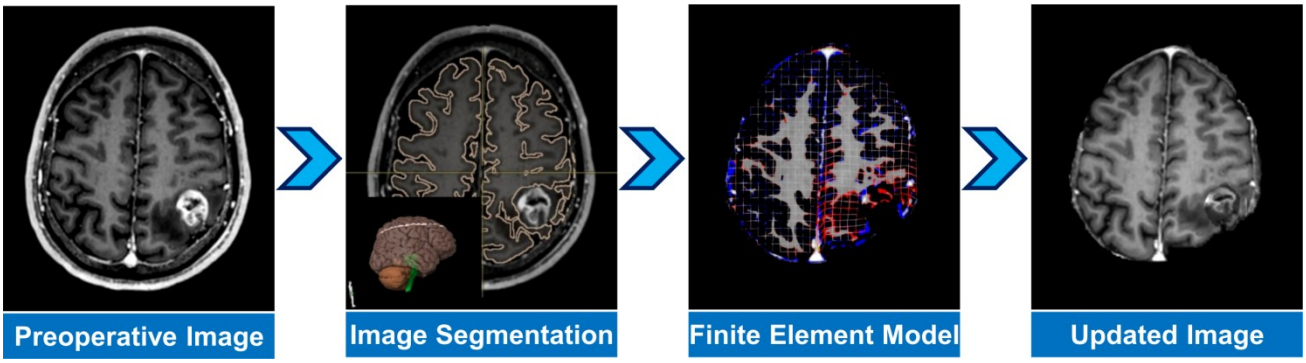

Figure 4: The main steps of IBEF

Preoperative images are automatically segmented based on brain atlas model to differ the soft and stiff tissues. Finite element model analysis is utilized to calculate collisions and deformations on segmented preoperative images to stimulate and update the preoperative images. The updated images are further fused with intraoperative images.

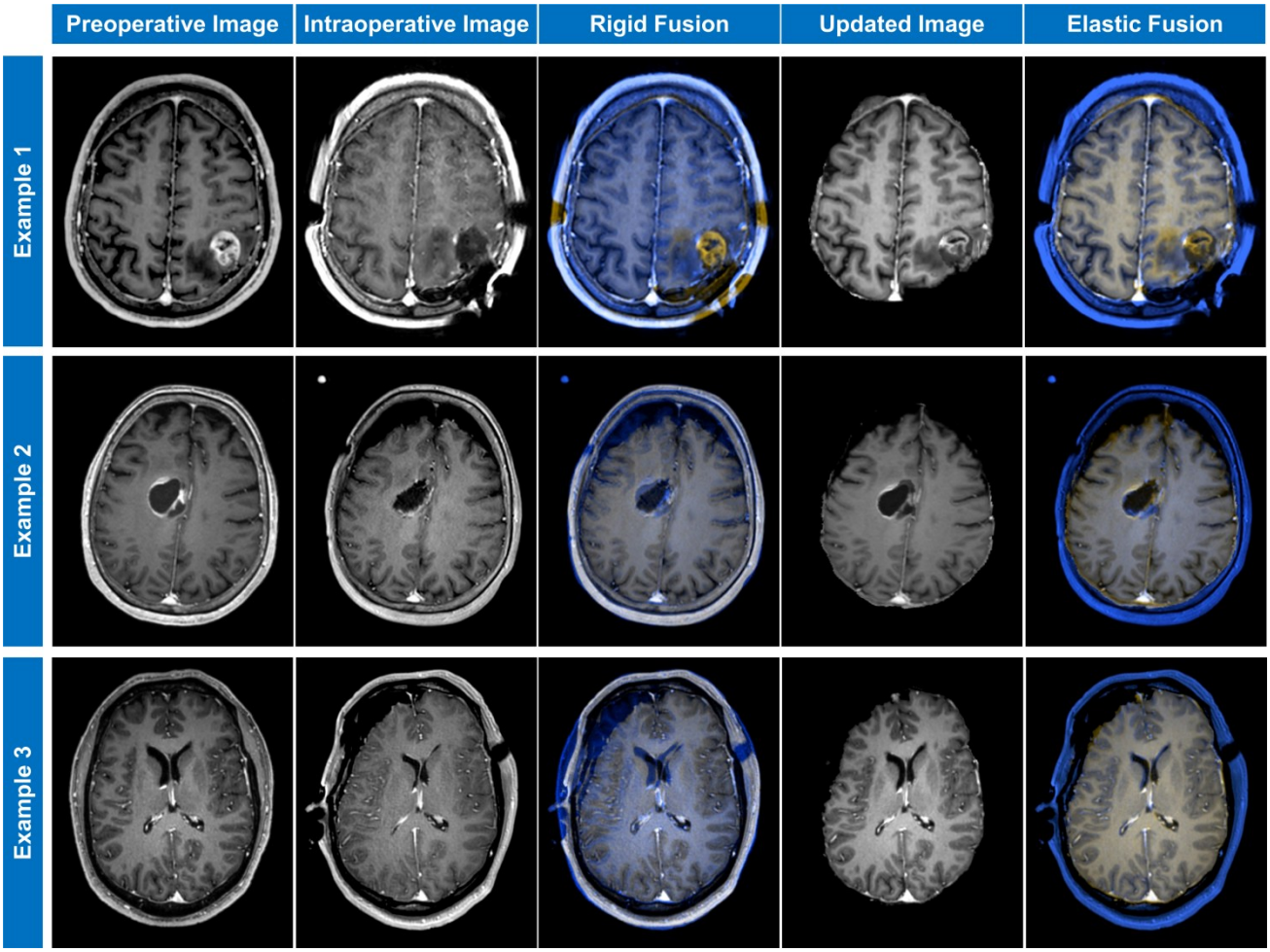

Figure 5: Examples of correction by IBEF

Rigid fusion of preoperative MRI and intraoperative MRI shows uncorrected registration. Preoperative MRI corrected by intraoperative MRI-based elastic fusion (IBEF) can better be matched with intraoperative images.

1.6 Previous Clinical Studies

The algorithm of IBEF mentioned above has been verified in a series of studies. In terms of compensation on anatomical structural images, Riva et al. evaluated the feasibility and performance of anatomical ioCT-based EF to update anatomical pMRI using clinical data, comparing the landmarks-based target registration error of RF with that of EF (Riva et al., 2019). The results illustrated that IBEF can improve the registration accuracy by 32% on average. Prior research reported by Negwer et al. shows a significant improvement in Euclidean distance of landmarks on

anatomical pMRI-ioMRI fused images from 2.67 ± 2.62 mm before IBEF to 1.80 ± 1.57 mm after the compensation of IBEF (Negwer et al., 2020).

For the updating of functional images, two previous studies analyzed the performance of IBEF on tractography compensation indirectly. DTI FT after the compensation of IBEF demonstrated a high correlation of intraoperative DES with clinical outcome. Intraoperative subcortical stimulations were performed in four cases by Ille et al. to confirm the site of the CST. In all cases after IBEF, the position of the CST as displayed by tractography matched the location detected by subcortical stimulation. (Ille et al., 2021a). Additionally, by analyzing the correlation between tumor-fibers distance and clinical outcomes in subcortical tumor resection, IBEF showed to offer a reliable modified FT intraoperatively for motor and language function (Ille et al., 2021b).

To sum up, the ability of IBEF to correct anatomical image misalignment caused by brain shift has been studied and demonstrated. However, a comprehensive comparison of IBEF to FT obtained from intraoperative DTI is still required.

Besides, the Euclidean distance of user-defined landmarks in two-dimensional space before and after IBEF was measured and compared to assess the performance of algorithm. This measurement is also a common metric to describe brain shift (Gerard et al., 2017). To reach high reliability, vessel bifurcations on recognizable features such as the carotid artery, the tip of basilar artery, middle cerebral artery, cortical vessel bifurcations, and contrast-enhancing structures were used as landmarks (Negwer et al., 2020; Riva et al., 2019). However, those easily recognizable structures did not exist on reconstructed fiber tracts. Since the difference in tractography morphology between intra- and preoperative FT is impacted by various parameters and artifacts, paired landmarks cannot be placed and repeated accurately on preoperative DTI tractography and intraoperative DTI tractography, respectively. It is necessary to regard fiber bundle as a 3D structure instead of defining two points that cannot be determined to pair. Metrics of spatial relationships can be utilized to

compare fused fiber tracts.

In theory, a variety of measurements may be used to evaluate 3D medical image segmentation (Taha & Hanbury, 2015). One option for evaluating the shift of fiber tracts is to measure the spatial relationship between two repeated segmentations. In neurosurgery, the spatial overlap index and the surface distance metric point by point are rarely applied. However, they are commonly used in the field of imaging evaluation. Those spatial measurements are suitable to be the comparison tools of 3D fiber tracts.

2. AIM OF THE STUDY

The aim of this study is to clarify if IBEF of preoperative tractography data can replace intraoperatively acquired DTI FT in a clinical setup.

This, the following hypotheses is proposed:

1) IBEF has the ability to correct the misalignment of preoperative DTI tractography when it severely affected by brain shift and does not overcorrect when tractography is not affected by brain shift.

2) Two reconstructed fiber bundles can be regard as 3D segmentations to be compared and evaluated by spatial measurements.

3. MATERIALS AND METHODS

The current study was conducted in conformity with the Helsinki Declaration. Prior to MR imaging, written consent was obtained from all participants. The study was approved by the local ethics board (registration number: 340/16 S, 336/17, 192/18, 18/19). The data analyzed in our study, including image scans acquired and surgeries, were part of the standard diagnosis and therapy required for regular medical practice. Processing of data analysis was fully anonymous.

3.1 Patients Data

This study retrospectively analyzed data from patients, who routinely performed pMRI, ioMRI, and underwent supratentorial tumor resection between February and November 2018. The quality of preoperative and intraoperative DTI data was comparable in voxel size, b-value, and diffusion gradient directions, and only a few artifacts or distortions were observed.

3.2 MRI Scanner

Preoperative MRI imaging including DTI sequences (b-value = 1000 s/mm^2, 32 diffusion gradient directions, thickness = 2.0 mm) were obtained prior to surgery (Philips Achieva 3.0T). IoMRI (Philips Ingenia 3.0T), including intraoperative DTI sequences with identical parameters of b-value, diffusion gradient directions, and layer thickness as preoperative DTI sequence, were acquired for all patients to verify the extent of resection.

3.3 Data Processing

To generate comparable fiber bundles, a data processing workflow was established and implemented in all patients' data (Figure 6). Anatomy-based DTI FT was performed on pre- and intraoperative MRIs separately. The rigidly fused image set of preoperative structural MRI and DTI fiber tracts was renovated by IBEF to obtain compensated DTI tractography. The image fusion of

compensated DTI tractography and intraoperative structural MRI were referred to as elastic fusion. Intraoperative DTI FT was used as a baseline to separately fuse the original and updated preoperative DTI FT. The spatial relationships of fiber tracts under RF and EF were then compared. The same software package was used for each step of data processing to ensure consistency in registration (Brainlab Elements®, version 3.1.0, Brainlab AG, Munich, Germany).

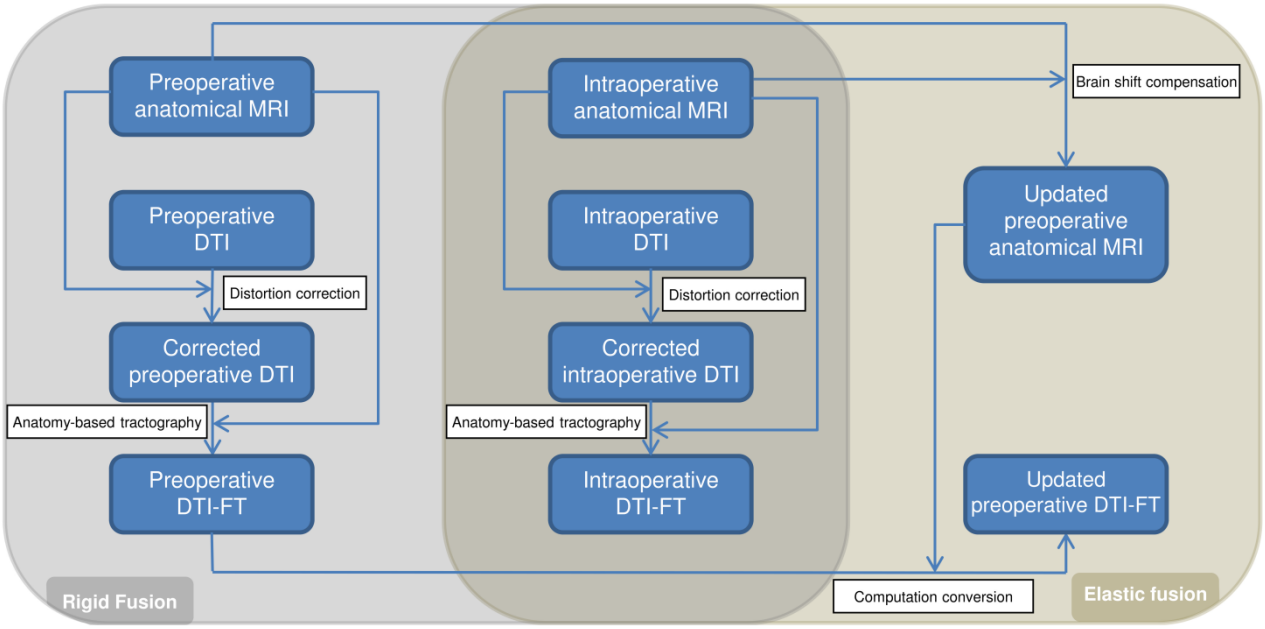

Figure 6: Flowchart for tractographies comparison of rigid and elastic fusion

This figure shows the flowchart including anatomy-based diffusor tensor imaging (DTI) fiber tracking (FT) being reconstructed on preoperative magnetic resonance imaging (MRI) and intraoperative MRI. The fusions of preoperative and intraoperative tractography were performed before and after intraoperative MRI-based elastic fusion. The differences in spatial relations of fused fiber tracts were statistically analyzed.

3.4 Distortion Correction

During the acquisition of diffusion MRI data, which is prone to distortion, echo planar imaging (EPI) provides the underpinning method (Albi et al., 2018; Gerhardt et al., 2019; Taylor et al., 2016). EPI is the fastest imaging acquisition method which can detect water motion. EPI distortion - as also known

as eddy current distortion - is induced by the inhomogeneity of magnetic fields (B0) and frequently occurs around the frontal and temporal pole, and the subarachnoid space. In the clinical application and data analysis, this nonlinear geometric distortion needs to be corrected to increase the estimation of DTI and the precision of FT (Albi et al., 2018; Taylor et al., 2016). A specific correction tool for current distortion (Distortion Correction Cranial, Brainlab Elements®, Brainlab AG, Munich, Germany) was evaluated in clinical settings previously. The results show that this approach can significantly improve the fusion accuracy between DTI and 3D anatomical MRI (Gerhardt et al., 2019). In the present study, this tool was applied for co-registration and correction of B0 images from preoperative and intraoperative DTI datasets with conventional anatomical MRI data for all cases (Figure 7).

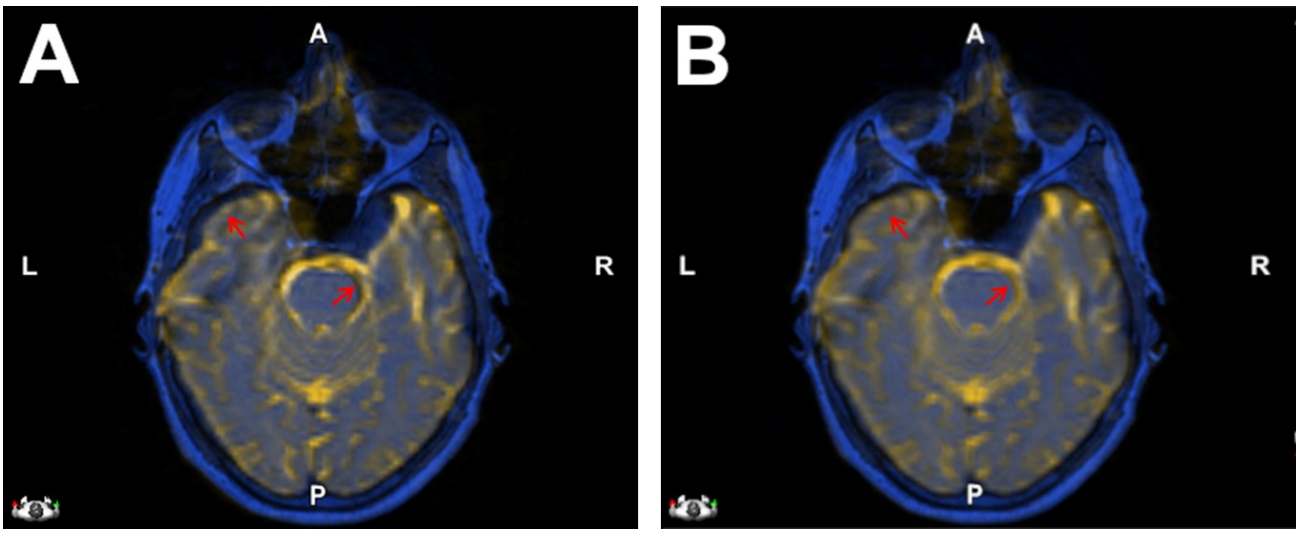

Figure 7: Images fusion of B0 and T1-weight before and after distortion correction

Image fusion of B0 image and anatomical image shows misalignment clearly being present around the cisterna ambiens and subarachnoid space (red arrow) before correction (Figure A). DTI sequence can partly be corrected to increase the precision of image fusion after distortion correction (Figure B).

3.5 Anatomy-based DTI Tractography

To assess the ability of IBEF in compensating for the displacement of fiber tracts, corticospinal tract (CST) and arcuate fasciculus (AF) were reconstructed in the present study. The CST is known as the

primary motor pathway for voluntary movements. The CST connects the motor cortex and the spinal cord (Schieber, 2007). AF is regarded as one of the critical tracts for language processing, which connects Broca's region, Wernicke's region, and Geschwind's region (Catani et al., 2005). Those tracts have been extensively studied as clinically important structures in tumor resection of motor- and language-eloquent regions (Frey et al., 2012; Negwer et al., 2017; Rosenstock et al., 2017; Sollmann et al., 2016; Weiss et al., 2015).

The precision of DTI FT can be improved by combining deterministic tractography with a multi-region-of-interest (ROI) method (Huang et al., 2004; Mori & van Zijl, 2002; Rosenstock et al., 2017). Fiber assignment by continuous tracking (FACT) is one of the common algorithms for deterministic tractography. The present study applied FACT to reconstruct fiber tracts (Fibertracking, Brainlab Elements®, Brainlab AG, Munich, Germany). The protocol of tractography consisting of four ROIs was used for CST FT (Figure 8A): Two subcortical ROIs were placed underneath the precentral gyrus and at the homolateral cerebral peduncle level (Frey et al., 2012; Weiss et al., 2015). To improve tracking quality of CST, the third and fourth ROIs were separately seeded at the level of the pons and the medulla (above the pyramidal cross line) on color-coded FA maps to exclude the transverse fibers (Rosenstock et al., 2017).

Several different protocols of parameters to perform DTI-derived CST tractography are described in the literature (Frey et al., 2012; Giordano et al., 2015; Sollmann et al., 2018b; Weiss et al., 2015). In this study, all reconstructed CST were performed under the same protocol (maximum angulation = 30°, minimum fiber length (MFL) = 110 mm, fractional anisotropy (FA) value = 75% fractional anisotropy threshold (FAT)). As a standardized protocol, these parameters are frequently utilized in prior research (Rosenstock et al., 2017; Sollmann et al., 2016; Sollmann et al., 2018b; Weiss et al., 2015). The FAT, which is defined as the maximum FA of only one fiber passing through all ROIs (Frey et al., 2012; Sollmann et al., 2018b), was determined individually. Meanwhile, two fixed FA

values (0.10 and 0.15) were added for CST tractography to reduce the deviations in FT quality caused by differing FA values (Figure 9 A1-A3).

An approach of three ROIs was used for AF tractography (Figure 8B). The first ROI was seeded in Broca's area, specifically in the white matter of Brodmann area (BA) 44, 45 and the surrounding cortex. The second ROI was placed at the subcortical level underneath the regions of superior and middle temporal gyri including Wernicke's area (BA 41, 42, 21, 22, 37), and the inferior parietal cortex, as known as Geschwind's area (BA 39, 40) (Catani et al., 2005; Glasser & Rilling, 2008). The last ROI was seeded - based on the coronal view of color-coded FA map - on the lateral side of internal capsule, hereby including all arcuate fibers in an anterior-posterior direction (Glasser & Rilling, 2008). Tractography with interval FA values of 25% FAT and 50% FAT, a maximum angulation of 30°, and an MFL of 110mm were performed in all cases of AF tracking (Figure 9 B1, B2). These parameters were previously utilized effectively in prior study (Sollmann et al., 2016).

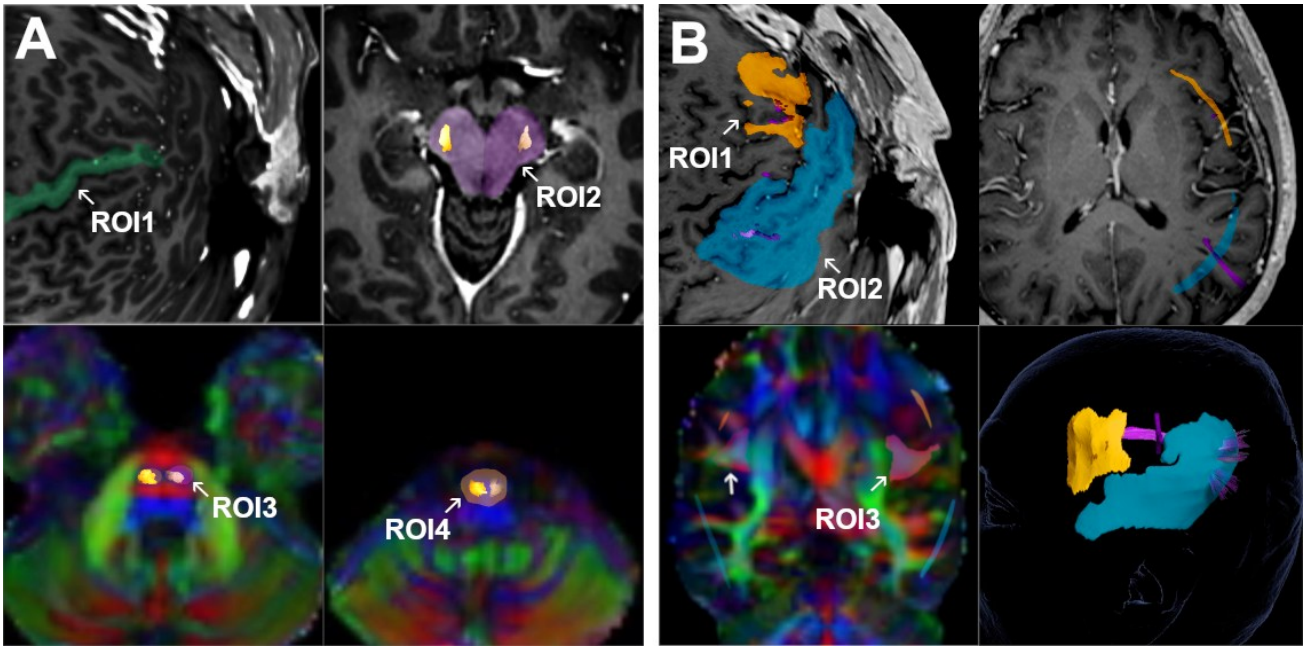

Figure 8: Anatomy-based FT of CST and AF with multi-ROI approach

The figure demonstrates the ROIs placement for the reconstruction of corticospinal tract (CST) and arcuate fasciculus (AF). For CST fiber tracking (FT) (Figure A), two regions of interest (ROI) were seeded

on color-coded FA maps at the pons and medulla levels (ROI 3, ROI4). Another two ROIs were placed at the midbrain level (ROI 2) and at the subcortical level beneath the precentral gyrus (ROI 1). For AF FT (Figure B), one ROI was set on the coronal view of color-coded FA maps on the longitudinal fiber's lateral side (ROI 3). The other two ROIs were placed - based on structural images - in the white matter of Broca's territory (ROI 1), and on the subcortical level of inferior parietal cortex, superior and middle temporal gyrus including Geschwind's territory and Wernicke's territory (ROI 2).

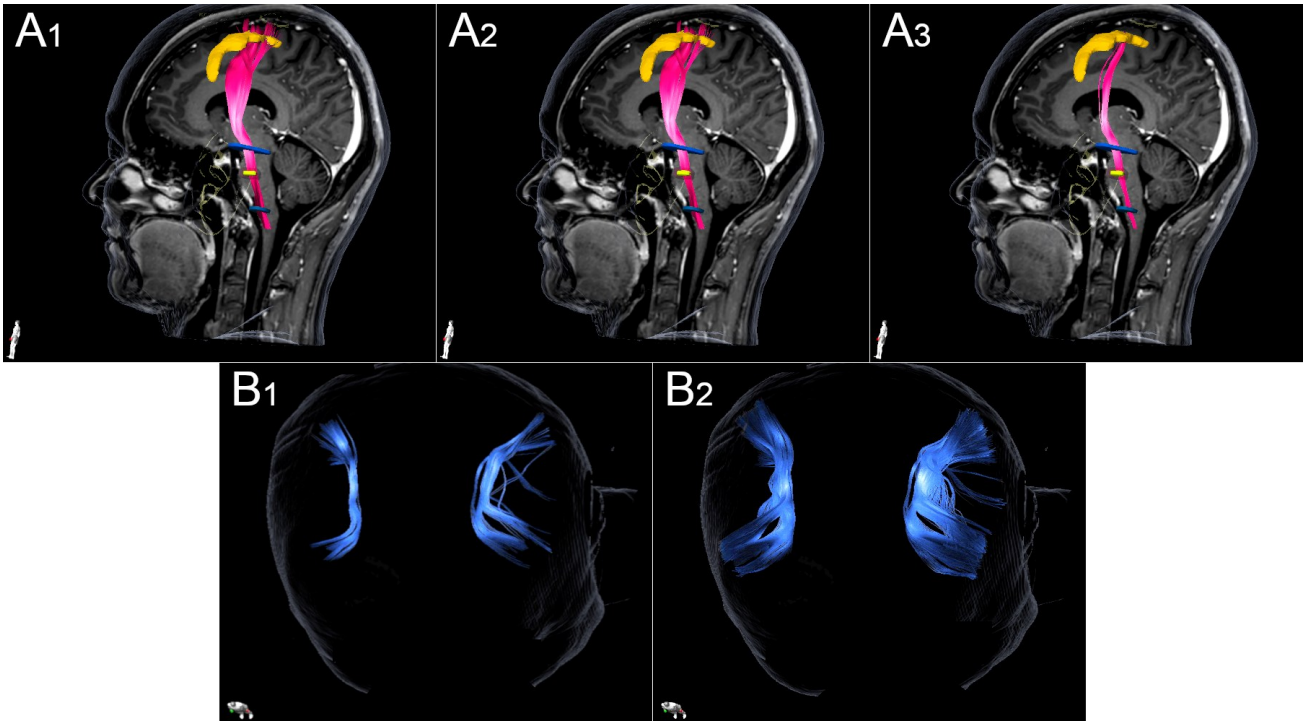

Figure 9: DTI FT performed in different FA values

To minimize the deviation of fiber tracking (FT) quality caused by different fractional anisotropy *(FA) values, tractography of the corticospinal tract was performed with FA=0.10 (Figure A1), FA=0.15 (Figure A2), and FA=75% FA* threshold *(FAT) (Figure A3). Tractography of the arcuate fasciculus (AF) was also performed individually with different FA values of 50% FAT (Figure B1) and 25% FAT (Figure B2).*

3.6 Standard Rigid Fusion and ioMRI-based Elastic Fusion

The pMRI and ioMRI datasets were fused using the typical RF approach, which includes conventional anatomical MRI images, DTI sequences corrected for distortion, and tractography that

tracked at the identical FA value (Image Fusion, Brainlab Elements®, Brainlab AG, Munich, Germany). Preoperative and intraoperative fiber bundles were rigidly fused and further analyzed (Figure 10). The resection cavity was manually delineated three-dimensionally in the surgery planning software using anatomical ioMRI to exclude it from the EF process (SmartBrush, Brainlab Elements®, Brainlab AG, Munich, Germany). The anatomical deformation between pMRI and ioMRI was calculated using the IBEF approach (Virtual iMRI, Brainlab Elements®, Brainlab AG, Munich, Germany). Based on the computation, the pMRI and preoperatively identified fiber tracts were corrected. The ioMRI was then merged with this newly generated imaging dataset. The spatial relationship between preoperative and intraoperative fiber tracts was then statistically evaluated and compared before and after IBEF (Figure 11).

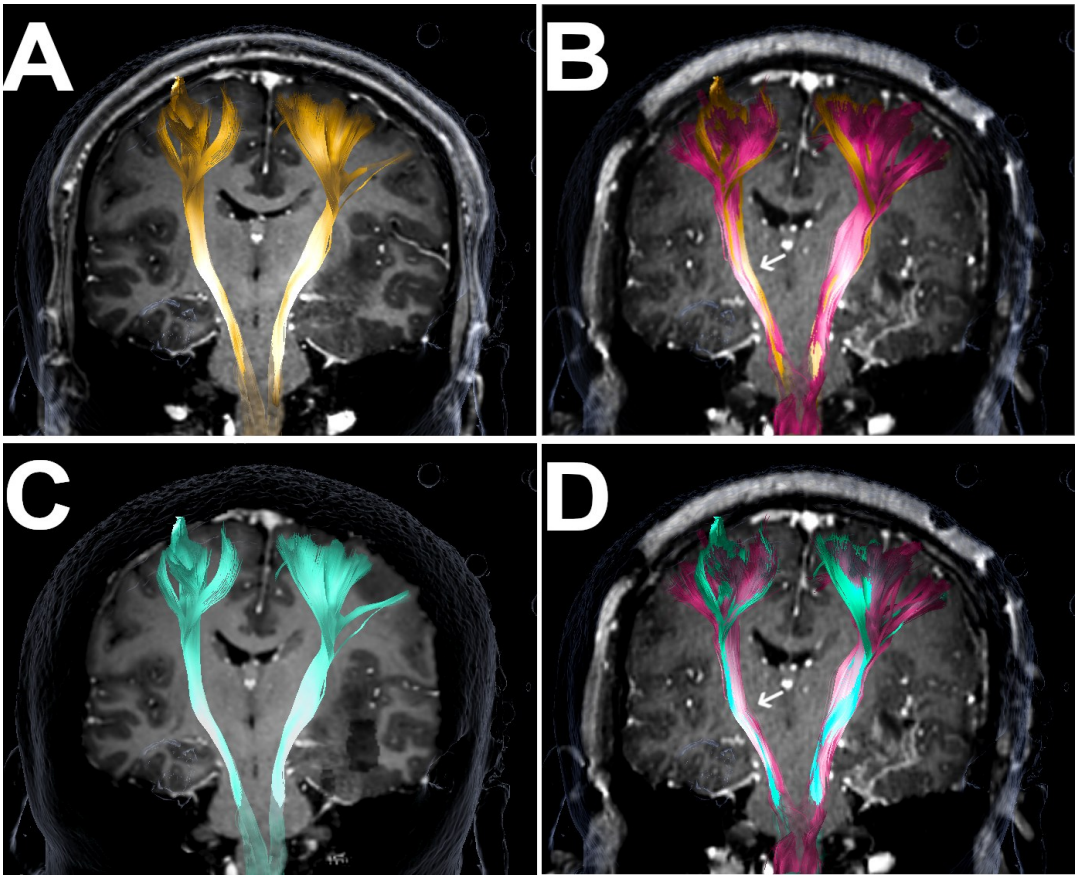

Figure 10: The image fusions of pre- and intraoperative CST fiber tracts before and after IBEF

This figure shows the anatomy-based corticospinal tract (CST) fiber tracking (FT) on preoperative magnetic resonance imaging (pMRI) and intraoperative MRI (ioMRI). Preoperative CST FT (yellow) is

demonstrated on pMRI (Figure A). The spatial relationship between intraoperative CST FT (pink) and preoperative CST FT is shown on ioMRI (Figure B). After the process of ioMRI-based elastic fusion (IBEF), updated preoperative CST FT (cyan) demonstrated on pMRI (Figure C) were generated and compared with intraoperative FT of the CST (pink) on ioMRI (Figure D).

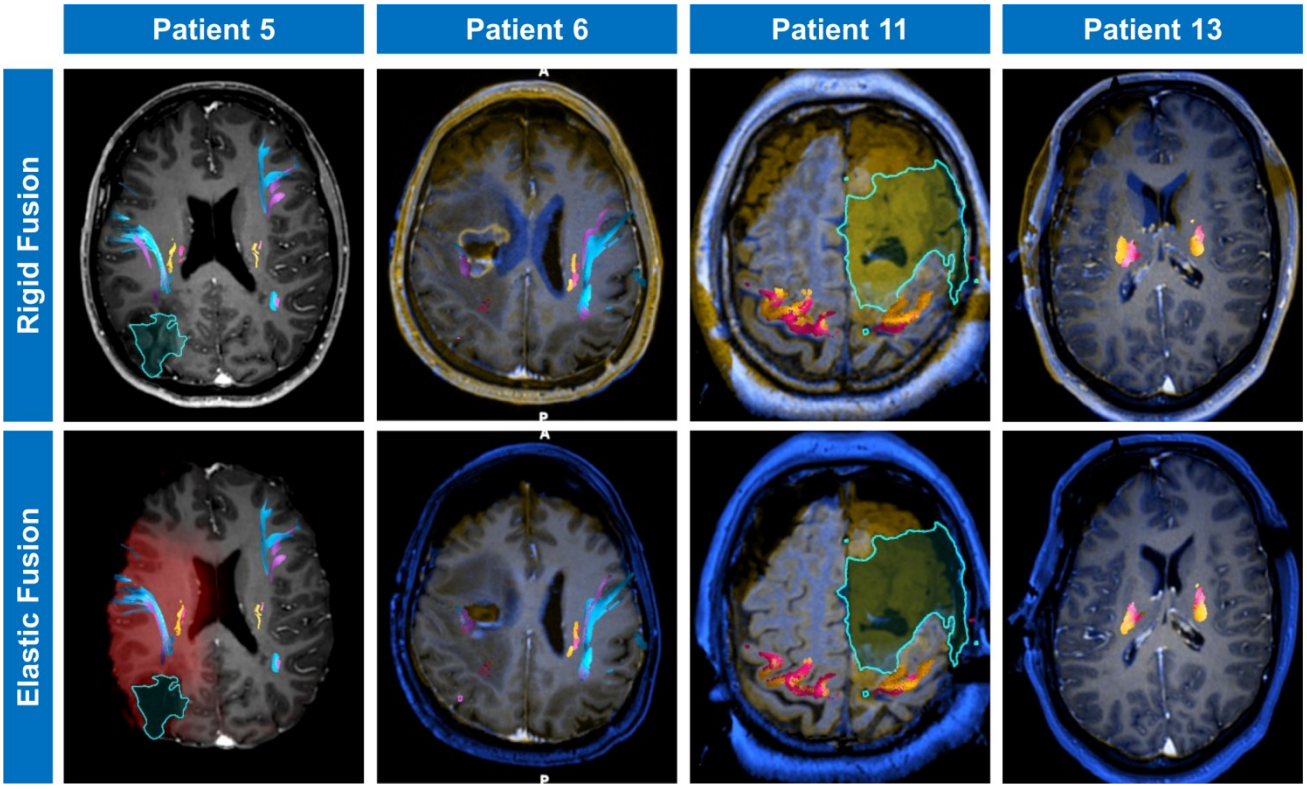

Figure 11: The demonstration of preoperative tractography before and after IBEF

Preoperative corticospinal tract (CST) fiber tracking (FT) (gold) and intraoperative CST FT (red), as well as preoperative arcuate fasciculus (AF) FT (purple) and intraoperative AF FT (blue), are compared after rigid fusion and elastic fusion, respectively. The figures demonstrate that fiber bundles can be fused better after the correction by intraoperative MRI-based elastic fusion (IBEF).

3.7 Data Analysis

3.7.1 Quantitative evaluation

The spatial relationship of two fused fiber bundles was quantified using Dice similarity coefficient (DICE), as well as the average surface distance (ASD) and Hausdorff distance (HD).

3.7.1.1 Dice similarity coefficient and average surface distance

DICE measures the overlapping volume of two segmented structures. It is a spatial overlap index that ranges from 0 to 1, denoting the range from none to total intersection (Taha & Hanbury, 2015; Zou et al., 2004). DICE is defined as

$$D = 2|A \cap B|/(|A| + |B|)$$

where |A| is indicated as a comparative or tested structure, which is the volume of the preoperative fiber bundle in the present study. |B| is defined as a reference or target structure, which is the volume of the intraoperative fiber bundle in the current analysis (Figure 12).

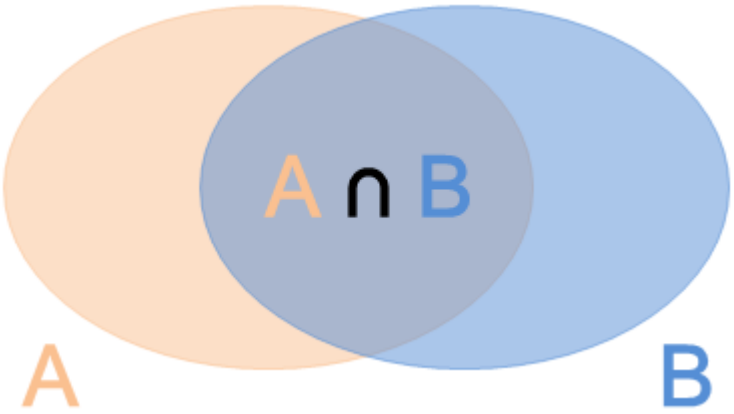

Figure 12: The diagram of Dice Coefficient

The surface points of two segmentations are used to generate ASD. The surface distance is the shortest distance between any arbitrary surface point in segmentation A and all surface points in segmentation B. In the interest of symmetry, the procedure is repeated from B to A. The process is defined as

$$D_B(a) = \min_{b \in B} \|a - b\| \text{ , and } D_A(b) = \min_{a \in A} \|b - a\|$$

where $\|.\|$ indicates Euclidean distance (Heimann et al., 2009). The formulation of ASD is

$$ASD(A, B) = \frac{1}{|A|+|B|}\left[\sum_{a \in A} D_B(a) + \sum_{b \in B} D_A(b)\right]$$

where |A| is the set of all preoperative fiber bundle surface points, and |B| is regarded as the collection of all points on the surface of intraoperative fiber bundle (Figure 13).

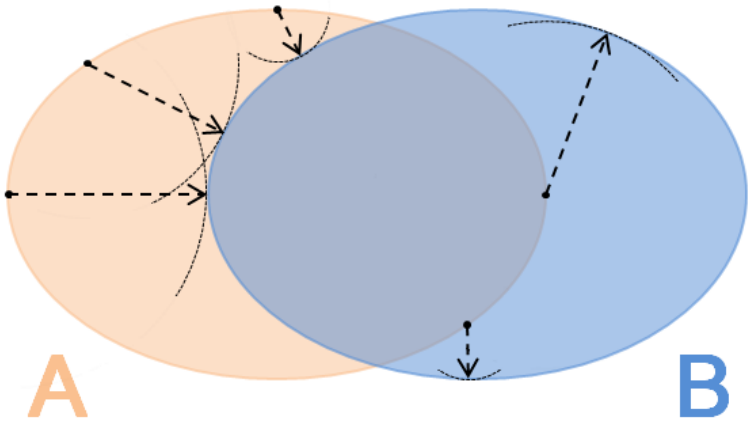

Figure 13: The diagram of surface distance

This figure demonstrates the definition of surface distance. The shortest distance from surface points (black dot) in structure A to the surface of structure B is the radius (dotted arrow) of a circle with the black dot as its center and tangent to B.

3.7.1.2 Hausdorff distance

Furthermore, another metric called Hausdorff distance (HD) can also be assessed to evaluate and compare pre- and intraoperative tracts, which is also a common metric for evaluating 3D medical image segmentations (Taha & Hanbury, 2015). HD is a spatial distance-based metric. Similar to ASD, the surface distance between structure A (comparison fiber bundle) and structure B (reference fiber bundle) is calculated. In the interest of symmetry, the procedure is also repeated from B to A. The difference is that HD returns the maximum value of all minimum surface distance, which is defined as

$$h(A,B) = \max_{a \in A} \min_{b \in B} \|a - b\| \text{ , and } h(B,A) = \max_{b \in B} \min_{a \in A} \|b - a\|$$

where $\|.\|$ indicates Euclidean distance, and

$$HD = \max \{h(A,B), h(B,A)\}$$

3.7.2 Statistical analysis

For DICE, ASD, and HD calculation, an internal measure tool evaluated and provided by Brainlab AG was utilized. The analysis is automatically calculated when two data sets of compared structures are loaded in the tool. The results were separately acquired from the background data of biomechanical modeling following RF and EF.

The data was separated into two categories: operated and non-operated hemispheres. The operated hemispheres are exposed to brain shift in a greater extent because of the craniotomy and resection of the lesion, while the brain tissues in the non-operated hemispheres were relatively stable in position. GraphPad Prism (version 9.0, GraphPad Software Inc., San Diego, CA, USA) was used to calculate the median ± interquartile range (IQR) for statistic description. The Wilcoxon rank test was performed to evaluate the difference in DICE, ASD, and HD of the paired samples in each group because of small sample sizes and due to parts of the data being non-normal distributed as indicated by Shapiro-Wilk test. The p-value threshold for statistical significance was set at $p=0.05$.

4. RESULTS

4.1 General Information

(The contents of the present section have been published with following title:
Wei Zhang, Sebastian Ille, Maximilian Schwendner, Benedikt Wiestler, Bernhard Meyer, Sandro M. Krieg. Tracking motor and language eloquent white matter pathways with intraoperative fiber tracking versus preoperative tractography adjusted by intraoperative MRI-based elastic fusion. J Neurosurg. Feb 25 2022:1-10. doi:10.3171/2021.12.JNS212106)

This study analyzed 17 patients with supratentorial brain tumors. Due to one case with a midline glioblastoma requiring craniotomy and tumor resection on both hemispheres, 18 hemispheres were divided into the group of operated hemispheres (GO), 16 hemispheres were divided into the group of non-operated hemispheres (GNO) (Zhang et al., 2022). The volume of the resection cavity had a median of 43.1 cm^3 (6.9 cm^3 - 164.1 cm^3) (Zhang et al., 2022). The ioMRI-related intraoperative procedure lasted for a median of 48 minutes (37 min - 85 min) (Zhang et al., 2022).

Except for one case in the GO, in which the software failed to acquire the CST FT at the FA level of 0.15 since the individual's FAT was less than 0.15 both on pre- and intraoperative tractography, DTI FT was successfully accomplished for the CSTs at FA values of 0.1, 0.15, and 75 % FAT in all hemispheres.

With regards to the AFs, 14 fiber tracts were documented in the GO, however, AF tractography were not traceable in four cases because the pathway of fiber tracts was located in or near the resection cavity (Zhang et al., 2022). In the GNO, 14 FT results were documented due to two cases not being properly traced, with one case in which the AF could not be identified and another one case that the intraoperative DTI data was of low quality (Zhang et al., 2022) (Table 1). In terms of ASD and HD analysis, two cases from the GO and one case from the GNO were removed due to surface distance values of greater than 50 mm, which were regarded as outliers to be excluded from further statistical analysis (Zhang et al., 2022) (Table 2).

Table 1: Patient characteristics

No.	Gender	Age	Pathology	Tumor location	Side	Resection cavity (cm^3)	Duration of ioMRI (min)	Operative position	Preop-FAT(left/right)		Intraop-FAT(left/right)	
									CST	AF	CST	AF
1	Male	53	HGG	Parietal	R	7.1	85	Prone	0.35/0.34	0.27/0.20	0.32/0.31	0.22/0.13
2	Male	59	HGG	Frontal	L, R	105.3	60	Supine	0.38/0.41	0.16/0.27	0.37/0.37	0.20/0.18
3	Female	68	HGG	Frontal	R	164.1	37	Supine	0.36/0.33	0.33/0.27	0.28/0.25	0.21/—
4	Male	65	Metastasis	Temporal	L	6.9	50	Right lateral	0.26/0.31	0.17/0.15	0.34/0.37	0.16/0.13
5	Female	38	LGG	Parieto-Occipital	L	26.4	46	Prone	0.38/0.38	0.13/0.29	0.42/0.35	0.09/0.27
6	Male	60	Metastasis	Frontal	L	43.7	48	Supine	0.11/0.35	0.10/0.19	0.12/0.42	0.15/0.20
7	Male	28	LGG	Fronto-Temporal	R	43.1	48	Supine	0.29/0.30	0.22/0.39	0.41/0.33	0.27/0.17
8	Female	76	HGG	Frontal	R	30.4	45	Supine	0.22/0.16	0.10/0.07	0.18/0.15	0.10/0.18
9	Male	41	HGG	Frontal	R	58.2	42	Supine	0.44/0.21	— /—	0.44/0.30	— /—
10	Female	35	LGG	Temporal	L	69.2	50	Supine/head to the right	0.25/0.36	0.32/0.27	0.29/0.25	0.17/0.14
11	Male	60	LGG	Frontal	R	141.8	45	Supine	0.28/0.29	0.24/—	0.27/0.28	0.14/—
12	Female	69	HGG	Frontal	L	13.7	48	Supine	0.29/0.22	0.25/0.20	0.36/0.26	0.28/—
13	Male	47	LGG	Temporal	L	21.5	50	Supine/head to the right	0.34/0.30	0.41/0.39	0.30/0.29	0.29/0.24
14	Male	53	HGG	Temporal	L	79.0	45	Supine/head to the right	0.23/0.36	0.17/0.12	0.25/0.42	0.22/0.27
15	Male	56	HGG	Frontal	L	35.2	41	Supine	0.31/0.37	0.16/0.12	0.34/0.34	0.17/0.23
16	Male	52	LGG	Frontal	R	120.2	50	Supine	0.27/0.28	0.31/0.13	0.27/0.18	0.22/0.07
17	Male	62	HGG	Frontal	L	34.5	38	Supine	0.25/0.37	— /0.29	0.28/0.36	— /0.29

This table shows patient characteristics of all 17 patients including gender, age, pathology of the tumor, location of the tumor, patient's position during surgery, duration of ioMRI-related surgical procedure, volume of the resection cavity and the fractional anisotropy threshold (FAT) of the corticospinal tract (CST) and arcuate fasciculus (AF) for each patient preoperatively and intraoperatively. (HGG: high-grade glioma; LGG: low-grade glioma)

4.2 Dice similarity coefficient and average surface distance

(The contents of the present section have been published with following title:
Wei Zhang, Sebastian Ille, Maximilian Schwendner, Benedikt Wiestler, Bernhard Meyer, Sandro M. Krieg. Tracking motor and language eloquent white matter pathways with intraoperative fiber tracking versus preoperative tractography adjusted by intraoperative MRI-based elastic fusion. J Neurosurg. Feb 25 2022:1-10. doi:10.3171/2021.12.JNS212106)

For fused CSTs before IBEF, the median value of DICE was 0.335 ± 0.140 in the group of operated hemispheres at an FA value of 0.10 (Zhang et al., 2022). The modified preoperative DTI FT at the same FA value of 0.10 exhibited enhanced spatial coherence and a considerable increase in terms of overlapped volumes with intraoperative DTI FT with a median of 0.395 ± 0.193 after IBEF ($p<0.001$) (Zhang et al., 2022). Similar findings appeared at FA values of 0.15 with a median of 0.300 ± 0.155 before IBEF and 0.390 ± 0.225 after IBEF ($p<0.001$). At the FA value of 75% FAT, a median of 0.185 ± 0.078 in DICE for RF and that of 0.210 ± 0.105 after IBEF were also obtained ($p=0.004$) (Zhang et al., 2022). At an FA value of 0.1 in the group of non-operated hemispheres, there was a smaller difference in DICE for fused CSTs before and after IBEF with median of 0.370 ± 0.153 and 0.385 ± 0.123($p=0.042$) (Zhang et al., 2022). There was no statistically significant improvement at the FA levels of 0.15 and 75% FAT (Zhang et al., 2022) (Table 2).

Similarly, in the GO, a substantial decrease in median values of ASD from 3.30 mm ± 2.53 mm before IBEF to 3.05 mm ± 2.15 mm after IBEF was obtained when FA value was 0.10 ($p<0.001$) (Zhang et al., 2022). Similar results were obtained for FA values of 0.15 with median values of ASD from 3.10 mm before IBEF, to 2.60 mm after IBEF ($p<0.001$), and from 3.90 mm to 3.70 mm when FA

value was 75% FAT (p=0.002) (Zhang et al., 2022). There were no statistical alterations in the GNO in any procedure (Zhang et al., 2022).

DICE values for AFs at 25% FAT showed no increase neither for the GO (p=0.086) nor for the GNO (p=0.410) (Zhang et al., 2022). With the FA value increased to 50% of individual FAT, however, substantial improvements were shown in the group of operated hemispheres after IBEF with the median value of DICE from 0.165 for RF to 0.195 after IBEF (p=0.012) (Zhang et al., 2022). No significant alterations were obtained in the non-operated hemispheres at an FA value of 50% FAT after IBEF (p=0.622) (Zhang et al., 2022). In terms of median values of ASD, at an FA value of 25% FAT, a non-significant reduction was achieved in the group of the operated hemispheres after IBEF (p=0.061), whereas a noticeable decrease was achieved at 50% FAT from 6.30 mm before IBEF to 5.30 mm after IBEF (p=0.012) (Zhang et al., 2022). There was no significant variation observed in the GNO at 25% FAT or 50% FAT (Zhang et al., 2022) (Figures 14 and 15).

Table 2: DICE and ASD statistical analysis of RF and IBEF

Group	Operated hemisphere					Non-operated hemisphere				
DICE [a.u.]	CST			AF		CST			AF	
FA	75% FAT (n=18)	0.15 (n=17)	0.10 (n=18)	50% FAT (n=14)	25% FAT (n=14)	75% FAT (n=16)	0.15 (n=16)	0.10 (n=16)	50% FAT (n=14)	25% FAT (n=14)
Rigid fusion	0.185 ±0.078	0.300 ±0.155	0.335 ±0.140	0.165 ±0.180	0.190 ±0.173	0.250 ±0.150	0.345 ±0.125	0.370 ±0.153	0.255 ±0.225	0.265 ±0.185
Elastic fusion	0.210 ±0.105	0.390 ±0.225	0.395 ±0.193	0.195 ±0.165	0.200 ±0.183	0.275 ±0.288	0.360 ±0.120	0.385 ±0.123	0.255 ±0.210	0.275 ±0.160
p-value	**0.004**	**<0.001**	**<0.001**	**0.012**	0.086	0.294	0.067	**0.042**	0.622	0.410

Group	Operated hemisphere					Non-operated hemisphere				
ASD [mm]	CST			AF		CST			AF	
FA	75% FAT (n=18)	0.15 (n=17)	0.10 (n=18)	50% FAT (n=12)	25% FAT (n=12)	75% FAT (n=16)	0.15 (n=16)	0.10 (n=16)	50% FAT (n=13)	25% FAT (n=13)
Rigid fusion	3.90 ±1.83	3.10 ±1.30	3.30 ±2.53	6.30 ±2.00	6.55 ±1.88	3.20 ±1.98	3.00 ±1.20	3.25 ±1.50	4.50 ±4.80	4.50 ±3.30
Elastic fusion	3.70 ±2.13	2.60 ±1.20	3.05 ±2.15	5.30 ±2.80	6.20 ±1.18	3.15 ±1.83	3.05 ±1.08	3.25 ±1.48	4.60 ±4.58	4.30 ±3.40
p-value	**0.002**	**<0.001**	**<0.001**	**0.012**	0.061	0.317	0.310	0.207	0.531	0.492

This table shows medians ± IQR and p-values of the dice coefficient (DICE) and the average surface distance (ASD) for the comparison of preoperative diffusion tensor imaging (DTI)-based tractography to intraoperative DTI-based tractography after rigid fusion (RF) and after intraoperative magnetic resonance imaging-based elastic fusion (IBEF). Corticospinal tract (CST), as well as arcuate fasciculus (AF), was

tracked under various levels of fractional anisotropy (FA) for the groups of operated and non-operated hemispheres. (a.u. = arbitrary unit; FAT= fractional anisotropy threshold)

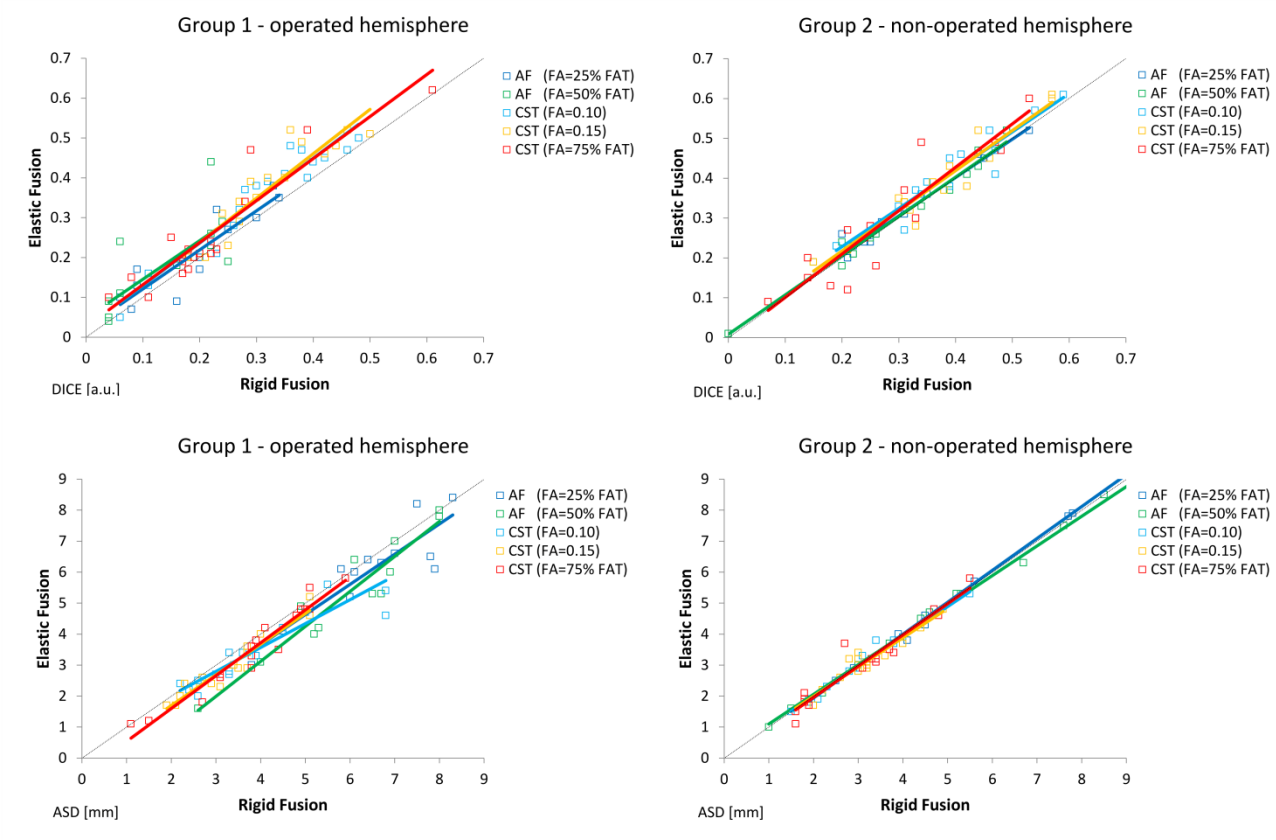

Figure 14: Scatter plots and linear regression trend line for DICE and ASD

The scatter plots show the results of the dice coefficient (DICE) and average surface distance (ASD) analyzed with and without the processing of intraoperative magnetic resonance imaging (ioMRI)-based elastic fusion for corticospinal tract (CST) and arcuate fasciculus (AF) at various values of fractional anisotropy (FA). (a.u. = arbitrary unit; FAT= fractional anisotropy threshold)

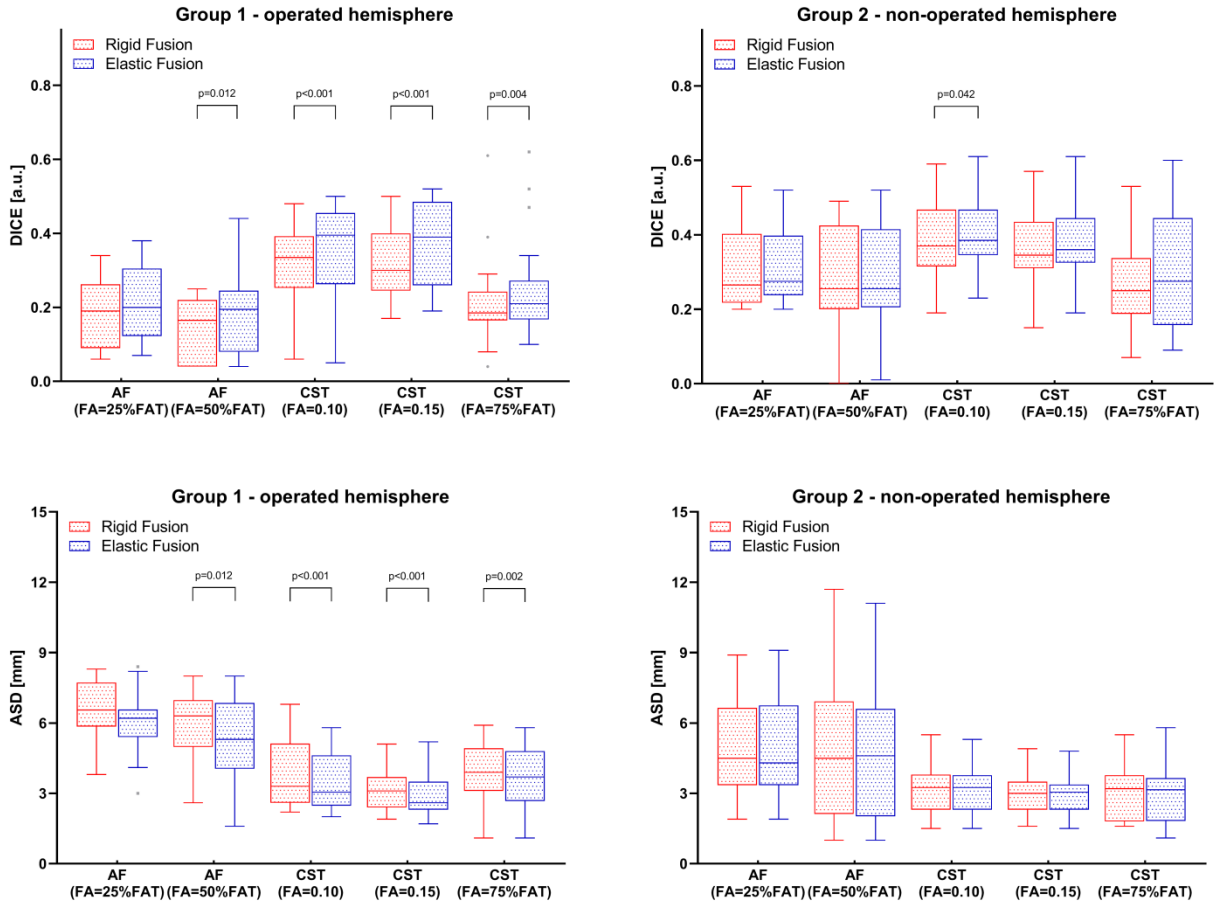

Figure 15: The box plots of DICE and ASD

The box plots show the results of dice coefficient (DICE), as well as average surface distance (ASD) analysis for corticospinal tract (CST) fiber tracking (FT) and arcuate fasciculus (AF) FT at different values of fractional anisotropy (FA) between rigid fusion and elastic fusion. (a.u. = arbitrary unit; FAT= fractional anisotropy threshold)

4.3 Hausdorff distance

In line with the results of ASD for the comparison of the CST FT, there was no statistical difference obtained in HD in any protocol in the GNO. However, in the GO, a non-significant decrease of median HD was found when the FA value was either 0.15 (p=0.534) or 75% FAT (p=0.112). A significant improvement was only achieved when FA value was 0.10 (24.60 mm ± 13.25 mm for RF vs. 24.50 mm ± 11.58 mm for IBEF, p=0.016).

Similarly, no significant decrease in HD was obtained in the GNO for the comparison of AF FT (FA=25% FAT, p=0.540; FA=50% FAT, p=0.723). Interestingly, even in the GO, there was no significant difference in HD at 25% FAT (p=0.350) and at 50% FAT (p=0.062) (Table 3, Figures 16 and 17).

Table 3: Statistical analysis of HD before and after IBEF

Group	Operated hemisphere					Non-operated hemisphere				
HD [mm]	CST			AF		CST			AF	
FA	75% FAT (n=18)	0.15 (n=17)	0.10 (n=18)	50% FAT (n=12)	25% FAT (n=12)	75% FAT (n=16)	0.15 (n=16)	0.10 (n=16)	50% FAT (n=13)	25% FAT (n=13)
Rigid fusion	23.10 ±12.98	20.10 ±8.80	24.60 ±13.25	29.45 ±14.00	32.05 ±8.40	21.70 ±9.73	24.90 ±10.58	25.00 ±11.70	27.40 ±14.95	24.90 ±12.05
Elastic fusion	22.60 ±12.03	20.20 ±11.20	24.50 ±11.58	29.20 ±12.70	30.80 ±15.00	21.25 ±8.73	24.15 ±10.75	24.80 ±11.18	27.70 ±14.43	24.00 ±11.90
p-value	0.112	0.534	**0.016**	0.062	0.350	0.111	0.624	0.105	0.723	0.540

This table shows medians ± IQR and p-values of Hausdorff distance (HD) for the comparison of preoperative diffusion tensor imaging (DTI)-based tractography to intraoperative DTI-based tractography before and after intraoperative magnetic resonance imaging-based elastic fusion (IBEF). The corticospinal tract (CST) fiber tracking (FT) and arcuate fasciculus (AF) FT at various levels of fractional anisotropy (FA) were tracked for the groups of operated and non-operated hemispheres. (FAT= fractional anisotropy threshold)

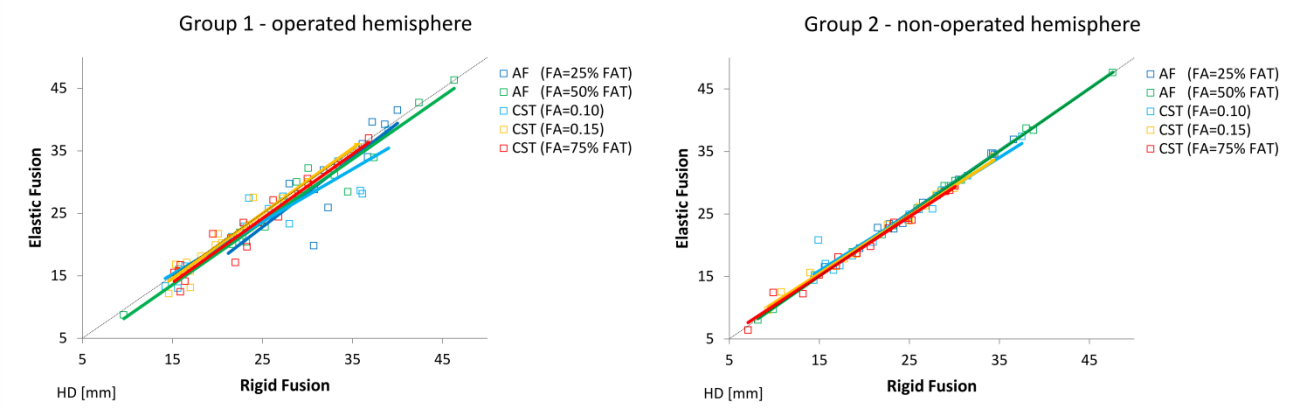

Figure 16: Scatter plots and linear regression trend lines for HD

The scatter plots show the results of Hausdorff distance (HD) analyzed before and after intraoperative magnetic resonance imaging-based elastic fusion. (FAT= fractional anisotropy threshold)

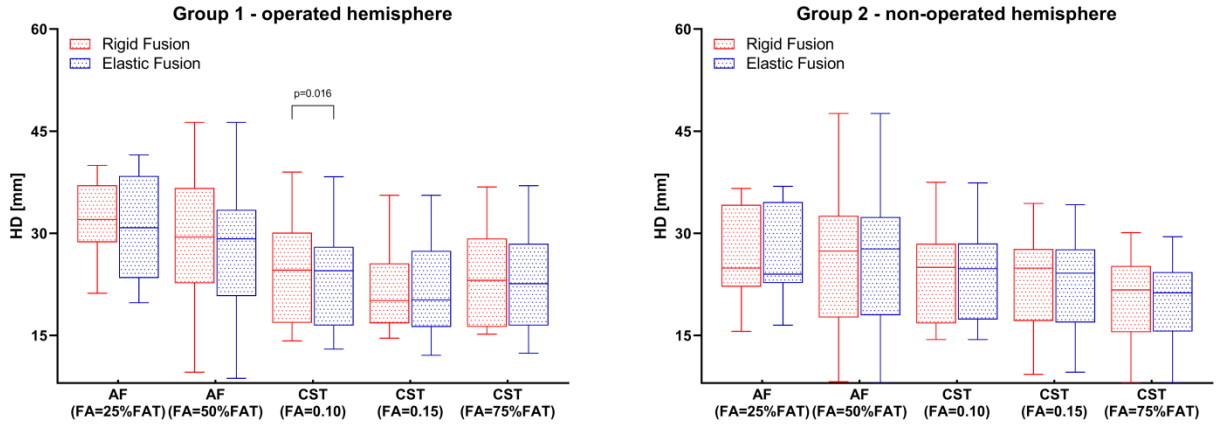

Figure 17: The box plots of HD

These box plots show the results of the Hausdorff distance (HD) analyzed before and after intraoperative magnetic resonance imaging-based elastic fusion for corticospinal tract (CST) fiber tracking (FT) and arcuate fasciculus (AF) FT at different values of fractional anisotropy (FA) between rigid fusion and elastic fusion. (FAT= fractional anisotropy threshold)

5. DISCUSSION

5.1 Comparison of Intraoperative DTI FT and Preoperative Tractography Before and After IBEF

In this study, when using intraoperative imaging dataset-based DTI FT as ground truth, preoperative tractography modified after IBEF improved the localization accuracy of FT compared to traditional RF. For all levels of FA values analyzed in the present evaluation, CST FT updated by IBEF demonstrated noticeable increases compared to RF in the features of overlapped volumes and surface distance. In the operated hemispheres, IBEF achieved a maximal improvement at an FA of 0.15, with the median value of ASD decreased by 0.50 mm for the CST. AF FT updated by IBEF yielded similar findings at an FA of 50% FAT, with the median value of ASD maximally decreased by 1.00 mm.

Riva et al. evaluate IBEF in terms of compensation for anatomical structure by defining anatomic landmarks in two groups: The landmarks in the operated hemispheres were regarded as test structures, while the landmarks in the non-operated hemispheres were regarded as control structures (Riva et al., 2019). Their results showed that the elastic fusion algorithm significantly improved the accuracy of navigation in the test structures, whereas the control structures were not changed by the algorithm (Riva et al., 2019). It can be concluded that this algorithm only acts where it is needed and keeps unaffected parts stable (Riva et al., 2019). In terms of tractography compensation, the present study yielded similar results in accordance with the report mentioned above. Remarkable improvements under various FA values were observed, especially within the operated hemispheres, while the localization of preoperative fiber tracts corrected by IBEF did not lead to overcompensation, when small-scale brain shifts occur in the non-operated hemispheres.

When analyzing similarity, DICE and ASD are strict methods highly sensitive to outliers. With this in

mind, correction by IBEF resulted in a significant improvement, suggesting that preoperative FT adjusted by IBEF is dependable and precise when compared to intraoperative DTI FT. According to the current study, IBEF appears to be a feasible approach for modifying visualized fiber tracts in accordance with intraoperative variations.

In accordance with the preoperatively traceable fiber tracts, intraoperative FT of the CSTs was acquired in 34 of 34 cases (100%) and intraoperative FT of the AFs were obtained in 28 of 30 cases (93.33%), showing a high proportion of success for intraoperative FT reconstruction (Zhang et al., 2022). The pre- and intraoperative CST FT locations were comparable and were all included in further analysis. However, 3 of 30 (10%) intraoperative AF tractographies were eliminated from further analysis due to substantial ASD displacement compared to preoperative tractographies (Zhang et al., 2022). In addition, for all FA levels, the difference between GO and GNO in terms of median ASD of AFs were greater than that of CSTs. Moreover, the statistically significant improvements of compensation can only be obtained on a small base of volume when the fiber bundle of the AF becomes narrower and constricted at an FA value of 50% FAT. The results indicate that a great gap between pre- and intraoperative AF fiber tracts challenges the maximum ability of IBEF. This also suggests that the AF is, to some extent, more easily impacted by brain shift than the CST.

5.2 Evaluation Metrics for the Shift of Fiber Tracts

In most cases, a target registration error based on anatomical landmarks is used to assess brain shift (Fan et al., 2018; Luo et al., 2017; Negwer et al., 2020; Riva et al., 2019). Euclidean distance of 16 landmark pairs before and after IBEF was measured by Negwer et al. Their results showed that it was significantly improved regardless of whether the landmark was independent or adjacent to the resection area (Negwer et al., 2020). The same method is used to measure the displacement of fiber tracts (Krivosheya et al., 2019; Nimsky et al., 2006). Nimsky et al. previously described using a

grid-scale to estimate the distance of tract shifts with a mean of 2.5 mm ± 5.8 mm (Nimsky et al., 2005). To measure the shift of tracts following the impact of tumor resection, a 3D measurement approach using shift radius was developed by Khalid et al. The shift radius was determined as the special distance between the anatomic landmarks on preoperative and postoperative images separately. The results illustrated the tracts shift on average from 2.72 mm at brainstem to 4.04 mm above the ventricles (Khalid et al., 2017). These methods are reliant on the placement of anatomical markers or manually placed points in two-dimensional space, which may lead to misalignment. Thus, objective, stringent, and quantitative comparison methodologies must be used to assess and measure the displacement of the fiber tracts.

For calculating the overlapped volume of similar image segmentations, DICE is a direct and representative measure (Zou et al., 2004). The present study validated the feasibility of measuring the overlap volume to evaluate the tracts' shift. The results of DICE between all fused fiber bundles were less than 0.4 even in the GNO with a slight shift, mainly due to morphological differences between pre- and intraoperative tractographies (Zhang et al., 2022). ASD is a spatial distance-based metric for the average shortest distance (Heimann et al., 2009). The shift distance of pre- and intraoperative CST fiber tracts is represented by a median ASD from 3.10 mm ± 1.30 mm to 6.55 mm ± 1.88 mm in the operated hemispheres, and from 3.00 mm ± 1.20 mm to 4.50 mm ± 3.30 mm in the non-operated hemispheres (Zhang et al., 2022). The results are in accordance with previous studies on the displacement distance of brain shift (Gerard et al., 2017).

ASD and HD are both calculated based on surface distance. However, the spatial metric of the greatest difference represented by HD is not suitable for the comparison of fiber bundles. As one of its main limitations, DTI can be impacted by several factors in diverse imaging situations and can lead to numerous artifacts, especially around the brain-air interface on the surface of exposed brain tissue and resection cavity intraoperatively. As a consequence, the local morphology of fiber bundles

can vary greatly, when compared between preoperative FT and intraoperative FT. The comparison of surface distance between pre- and intraoperative tractography results in a number of outliers. Unlike ASD which takes an average to minimize the impact of outliers, HD outputs the greatest outlier as a result and draws an unobjective conclusion, and therefore does not recommend applying for the measurement of tract shift.

5.3 Necessity of Tractography Adjusted by IBEF

In the past decades, ioMRI has been frequently utilized in neurosurgery, especially for brain tumor resection (Black et al., 1997; Khan et al., 2017; Kubben et al., 2011). Intraoperative MRI can update the image-guided neuronavigation and significantly increase the extent of resection (EOR) to approach gross total resection (GTR) (Hatiboglu et al., 2009; Napolitano et al., 2014; Shah et al., 2020). EOR is a modifiable factor that neurosurgeons can control. A higher EOR is considered to be an independent factor associated with prolonged overall and progression-free survival (Chaichana et al., 2014; Lacroix et al., 2001; Stark et al., 2012). However, GTR is no longer the sole purpose of neurosurgery, especially for malignant brain lesions. The concept, that preservation of function plays a key role, has become a consensus among neurosurgeons (Aghi et al., 2015; Young et al., 2015). The implementation of ioMRI should focus on functional protection and the improvement of quality of life, rather than only the pursuit of lesion resection. With this in mind, it is essential to precisely display functional areas and fiber bundles on the structural images of pre- and intraoperative imaging in order to guide a safe resection.

Tractography can be reconstructed based on intraoperative DTI combined with intraoperative mapping and neurophysiological monitoring. However, significant restrictions need to be faced, particularly with regard to the scanner limiting the acquisition of intraoperative DTI and the quality of FT (Maesawa et al., 2010; Munnich et al., 2019). The reconstruction of fiber tracts is constrained by lower resolution when DTI is acquired in a low-intensity magnetic field ioMRI. Due to the resection

cavity with intraoperative application of saline and collagenous sponge, residual tumor, and surgery-related edema, additional artifacts will be generated in high-field ioMRI, especially in the surface of the exposed cortex, and in subcortical area as well (Ginat et al., 2014; Maesawa et al., 2010; Nimsky, 2011; Nimsky et al., 2005; Ostry et al., 2013; Vargas et al., 2009). Moreover, awake neurosurgeries with DES inevitably involve certain possible intraoperative complications, such as stimulation-related intraoperative seizures and respiratory depression and can lead to several undesirable psychological complications for patients (Conte et al., 2008; McAuliffe et al., 2018; Milian et al., 2013; Roca et al., 2019). A further limitation of DES entails that the identification of pathways can only take place when the stimulator is very close to the fibers. Direct cortical stimulation can only be performed on the exposed brain intraoperatively when reaching the margin of the resection cavity without a global view of fiber bundle distribution, which may neglect the size of major white matter tracts and potentially induce permanent deficits (Borchers et al., 2011). Hence, it is essential to perform brain shift compensation of whole fiber bundles as an integrated object and integrate it into the IGNS. In addition, the position of the craniotomy, the size of the bone flap, and the extent of the lesion can restrict the application of intraoperative stimulation, making preoperative functional mapping and tractography data the sole reference for functional areas and allowing it to play a significant role in tumor resection. These difficulties necessitate updated preoperative FT and the compensation of tracts shift, especially when intraoperative DTI FT is not achievable.

5.4 Limitations

DTI FT is a user-controlled procedure containing variables like angulations, MFL, and FA. A wide range of inaccuracies can likely occur because of the limits of DTI FT. Fiber tractographies vary in shape and size between intraoperative and preoperative FT, making comparisons of reconstructed fiber bundles in different situations difficult. More clinical experience is needed to test the EF approach of compensating for brain shift in order to continuously improve the accuracy of the

algorithm. Furthermore, the current study evaluated IBEF using anatomy-based tractography and lacked cortical function mapping data. To improve and validate the accuracy of IBEF, functional mapping tools, such as fMRI, nTMS, and even DES, might be used to further enhance tractography for evaluation. Moreover, and perhaps most crucially, the current data focused on comparing imaging data alone, without consideration of DES or clinical outcome metrics. This should be addressed in future studies in order to verify the reliability and usability of IBEF in clinical practice.

5.5 Conclusion

Preoperative FT impacted by obvious brain shift can be corrected by IBEF effectively in the operated hemispheres, while the EF process does not overcorrect the FT in the non-operated hemispheres. The present study clarified that preoperative FT updated by IBEF can replace intraoperatively acquired DTI FT in a clinical setup. Spatial similarity metrics such as DICE and ASD can be utilized to compare and evaluate the shift of fiber tracts.

6. SUMMARY

The present study evaluated the ability and performance of the algorithm of biomechanical model-based elastic image fusion for the compensation of misalignment in DTI FT induced by surgery-related brain shift in a clinical setting. The present study also demonstrated the feasibility of the method by comparing reconstructed pre- and intraoperative DTI fiber tracts with appropriate 3D spatial similarity measurements.

Currently, preoperative anatomical imaging combined with DTI FT provides neurosurgeons the vivid visualization of white matter pathways both in preoperative planning of the surgery and in the intraoperative resection procedure. However, the misalignment of preoperative images registration due to brain shift impairs the accuracy of image-guided neuronavigation systems (IGNS). Intraoperative tractography is often constrained by technical limitations of intraoperative acquisition of diffusion imaging, quality factors, and time restrictions. As a solution, biomechanical-modeling and intraoperative MRI-based elastic fusion (IBEF) provides an available approach to update preoperative tractography. The present study hypothesized that IBEF can correct the misalignment of preoperative DTI tractography and replace intraoperatively acquired DTI FT in a clinical setup.

To quantify and compare the fused fiber tracts, a set of 3D spatial similarity measurements consisting of DICE, ASD, and HD was introduced and utilized in the present study. CST and AF were reconstructed both on pMRI and ioMRI based on anatomical DTI FT at various FA values. Both rigid fusion (RF) and IBEF were performed for pre- and intraoperative tractographies in the group of operated and non-operated hemispheres. By comparing the differences in spatial relations of fused fiber tracts under RF and after IBEF when taking intraoperative DTI FT as reference, the results of DICE and ASD illustrated significant improvements in the overlap of volume and spatial distance after IBEF in the group of operated hemispheres, while HD was considered to be an inappropriate metric for the comparison of 3D fiber tracts.

In conclusion, preoperative FT updated by IBEF is comparable with intraoperative FT. The protocol of compensation for fiber shift can be an alternative to accurately visualize the tractography intraoperatively. With the ability of updating preoperative fiber tracts to compensate for the impact of brain shift and resection cavity, IBEF is able to provide an alternative approach of intraoperative functional navigation in neurosurgery practice and can replace the intraoperatively acquired DTI FT in a clinical setup when intraoperative functional imaging cannot be achieved.

7. ZUSAMMENFASSUNG

In der vorliegenden Studie wurde die Fähigkeit und Performance eines Algorithmus einer biomechanischen modellbasierten elastischen Bildfusion zur Kompensation eines Misalignments im DTI FT evaluiert, welches durch eine operationsbedingte Verlagerung des Gehirns in der klinischen Anwendung verursacht wird. Die vorliegende Studie zeigt weiterhin die Durchführbarkeit der Methode durch den Vergleich rekonstruierter prä- und intraoperativer DTI Faserbahnen mit geeigneten 3D Ähnlichkeitsmaß.

Aktuell stellt die präoperative anatomische Bildgebung in Verbindung mit DTI FT Neurochirurgen eine anschauliche Visualisierung der Bahnen der weißen Substanz sowohl bei präoperativer Planung des Eingriffs wie auch intraoperativ während der Resektion dar. Jedoch beeinträchtigt ein Misalignment der registrierten präoperativen Bilder aufgrund von Hirnverlagerung die Genauigkeit einer bildgestützen Neuronavigationssysteme. Intraoperative Traktographie wird oft eingeschränkt durch technische Limitationen einer intraoperativ erfassten Diffusionsbildgebung, Qualitätsfaktoren und zeitliche Restriktionen. Im Sinne einer Lösung bietet eine biomechanische Modellierung und eine elastische Fusion basierend auf einem intraoperativen MRT (IBEF) ein mögliches Konzept zur Aktualisierung der präoperativen Traktographie. Die Hypothese der Studie stellt dar, dass IBEF das Misalignment einer präoperativen DTI Traktographie korrigieren und intraoperativ erworbenes DTI FT zur klinischen Anwendung ersetzen kann.

Um die fusionierten Faserbahnen zu quantifizieren und zu vergleichen, wurde ein Set 3D räumlicher Ähnlichkeitsmaße, bestehend aus DICE, ASD und HD in der vorliegenden Studie verwendet. CST und AF wurden beide anhand des pMRI und ioMRI basierend auf das anatomische DTI FT mit unterschiedlichen FA-Werten rekonstruiert. Sowohl die rigide Fusion (RF) und IBEF wurden für prä- und intraoperative Traktographien in operierten und nicht-operierten Hemisphären durchgeführt. Im Vergleich der Abweichungen der räumlichen Beziehungen der fusionierten Faserbahnen nach RF

und IBEF mit dem intraoperativen DTI FT als Referenz, zeigte sich in den Resultation von DICE und ASD signifikante Verbesserungen bei Übereinstimmung von Volumen und räumlicher Entfernung nach IBEF in der Gruppe der operierten Hemisphären, wobei HD als ungeeignetes Maß zum Vergleich der 3D Faserbahnen angesehen wurde.

Zusammengefasst ist ein präoperatives FT, welches durch IBEF aktualisiert wurde, vergleichbar mit intraoperativem FT. Das Protokoll zur Kompensation eines Shifts der Faserbahnen kann eine Alternative darstellen zur akkuraten intraoperativen Darstellung der Traktographie. Mit der Fähigkeit, präoperativ bestimmte Faserbanen zur Kompensation der Wirkung der Hirnverlagerung und der Resektionshöhle zu aktualisieren, kann IBEF ein alternatives Konzept einer intraoperativen funktionellen Navigation im neurochirurgischen Alltag darstellen und die intraoperativ erworbene DTI FT in einem klinischen Setup ersetzen, wenn intraoperative funktionelle Bildgebung nicht möglich ist.

8. REFERENCES

Aghi, M. K., Nahed, B. V., Sloan, A. E., Ryken, T. C., Kalkanis, S. N., & Olson, J. J. (2015). The role of surgery in the management of patients with diffuse low grade glioma: A systematic review and evidence-based clinical practice guideline. *J Neurooncol*, *125*(3), 503-530. https://doi.org/10.1007/s11060-015-1867-1

Albi, A., Meola, A., Zhang, F., Kahali, P., Rigolo, L., Tax, C. M. W., . . . O'Donnell, L. J. (2018). Image Registration to Compensate for EPI Distortion in Patients with Brain Tumors: An Evaluation of Tract-Specific Effects. *J Neuroimaging*, *28*(2), 173-182. https://doi.org/10.1111/jon.12485

Alexopoulos, G., Cikla, U., El Tecle, N., Kulkarni, N., Pierson, M., Mercier, P., . . . Abdulrauf, S. (2019). The Value of White Matter Tractography by Diffusion Tensor Imaging in Altering a Neurosurgeon's Operative Plan. *World Neurosurg*, *132*, e305-e313. https://doi.org/10.1016/j.wneu.2019.08.168

Azagury, D. E., Dua, M. M., Barrese, J. C., Henderson, J. M., Buchs, N. C., Ris, F., . . . Visser, B. C. (2015). Image-guided surgery. *Curr Probl Surg*, *52*(12), 476-520. https://doi.org/10.1067/j.cpsurg.2015.10.001

Baciu, M., Le Bas, J. F., Segebarth, C., & Benabid, A. L. (2003). Presurgical fMRI evaluation of cerebral reorganization and motor deficit in patients with tumors and vascular malformations. *European Journal of Radiology*, *46*(2), 139-146. https://doi.org/10.1016/S0720-048X(02)00083-9

Barz, A., Noack, A., Baumgarten, P., Seifert, V., & Forster, M.-T. (2018). Motor Cortex Reorganization in Patients with Glioma Assessed by Repeated Navigated Transcranial Magnetic Stimulation–A Longitudinal Study. *World Neurosurgery*, *112*, e442-e453. https://doi.org/https://doi.org/10.1016/j.wneu.2018.01.059

Bayer, S., Maier, A., Ostermeier, M., & Fahrig, R. (2017). Intraoperative Imaging Modalities and Compensation for Brain Shift in Tumor Resection Surgery. *Int J Biomed Imaging*, *2017*, 6028645. https://doi.org/10.1155/2017/6028645

Bello, L., Gambini, A., Castellano, A., Carrabba, G., Acerbi, F., Fava, E., . . . Falini, A. (2008). Motor and language DTI Fiber Tracking combined with intraoperative subcortical mapping for surgical removal of gliomas. *Neuroimage*, *39*(1), 369-382.

https://doi.org/10.1016/j.neuroimage.2007.08.031

Benveniste, R. J., & Germano, I. M. (2005). Correlation of factors predicting intraoperative brain shift with successful resection of malignant brain tumors using image-guided techniques. *Surgical Neurology*, *63*(6), 542-548. https://doi.org/https://doi.org/10.1016/j.surneu.2004.11.025

Black, P. M., Moriarty, T., Alexander, E., 3rd, Stieg, P., Woodard, E. J., Gleason, P. L., . . . Jolesz, F. A. (1997). Development and implementation of intraoperative magnetic resonance imaging and its neurosurgical applications. *Neurosurgery*, *41*(4), 831-842; discussion 842-835. https://doi.org/10.1097/00006123-199710000-00013

Borchers, S., Himmelbach, M., Logothetis, N., & Karnath, H. O. (2011). Direct electrical stimulation of human cortex - the gold standard for mapping brain functions? *Nat Rev Neurosci*, *13*(1), 63-70. https://doi.org/10.1038/nrn3140

Brahimaj, B. C., Kochanski, R. B., Pearce, J. J., Guryildirim, M., Gerard, C. S., Kocak, M., . . . Byrne, R. W. (2021). Structural and Functional Imaging in Glioma Management. *Neurosurgery*, *88*(2), 211-221. https://doi.org/10.1093/neuros/nyaa360

Braun, V., Dempf, S., Tomczak, R., Wunderlich, A., Weller, R., & Richter, H. P. (2000). Functional cranial neuronavigation. Direct integration of fMRI and PET data. *J Neuroradiol*, *27*(3), 157-163. https://www.ncbi.nlm.nih.gov/pubmed/11104962

Bucholz, R., & McDurmont, L. (2009). The History, Current Status, and Future of the StealthStation Treatment Guidance System. In A. M. Lozano, P. L. Gildenberg, & R. R. Tasker (Eds.), *Textbook of Stereotactic and Functional Neurosurgery* (pp. 543-565). Springer Berlin Heidelberg. https://doi.org/10.1007/978-3-540-69960-6_36

Cao, A., Thompson, R. C., Dumpuri, P., Dawant, B. M., Galloway, R. L., Ding, S., & Miga, M. I. (2008). Laser range scanning for image-guided neurosurgery: investigation of image-to-physical space registrations. *Med Phys*, *35*(4), 1593-1605. https://doi.org/10.1118/1.2870216

Carl, B., Bopp, M., Saß, B., & Nimsky, C. (2018). Intraoperative computed tomography as reliable navigation registration device in 200 cranial procedures. *Acta Neurochirurgica*, *160*(9), 1681-1689. https://doi.org/10.1007/s00701-018-3641-6

Catani, M., Jones, D. K., & ffytche, D. H. (2005). Perisylvian language networks of the human brain. *Ann Neurol*, *57*(1), 8-16. https://doi.org/10.1002/ana.20319

Chaichana, K. L., Cabrera-Aldana, E. E., Jusue-Torres, I., Wijesekera, O., Olivi, A., Rahman, M., & Quinones-Hinojosa, A. (2014). When Gross Total Resection of a Glioblastoma Is Possible, How Much Resection Should Be Achieved? *World Neurosurgery*, *82*(1), e257-e265. https://doi.org/https://doi.org/10.1016/j.wneu.2014.01.019

Chua, T. H., See, A. A. Q., Ang, B. T., & King, N. K. K. (2018). Awake Craniotomy for Resection of Brain Metastases: A Systematic Review. *World Neurosurg*, *120*, e1128-e1135. https://doi.org/10.1016/j.wneu.2018.08.243

Coenen, V. A., Abdel-Rahman, A., McMaster, J., Bogod, N., & Honey, C. R. (2011). Minimizing brain shift during functional neurosurgical procedures - a simple burr hole technique that can decrease CSF loss and intracranial air. *Cent Eur Neurosurg*, *72*(4), 181-185. https://doi.org/10.1055/s-0031-1279748

Conte, V., Baratta, P., Tomaselli, P., Songa, V., Magni, L., & Stocchetti, N. (2008). Awake neurosurgery: an update. *Minerva Anestesiol*, *74*(6), 289-292. https://www.ncbi.nlm.nih.gov/pubmed/18500200

Daniel, A. G. S., Park, K. Y., Roland, J. L., Dierker, D., Gross, J., Humphries, J. B., . . . Leuthardt, E. C. (2021). Functional connectivity within glioblastoma impacts overall survival. *Neuro Oncol*, *23*(3), 412-421. https://doi.org/10.1093/neuonc/noaa189

Dubey, A., Kataria, R., & Sinha, V. D. (2018). Role of Diffusion Tensor Imaging in Brain Tumor Surgery. *Asian J Neurosurg*, *13*(2), 302-306. https://doi.org/10.4103/ajns.AJNS_226_16

Dumpuri, P., Thompson, R. C., Cao, A., Ding, S., Garg, I., Dawant, B. M., & Miga, M. I. (2010). A fast and efficient method to compensate for brain shift for tumor resection therapies measured between preoperative and postoperative tomograms. *IEEE Trans Biomed Eng*, *57*(6), 1285-1296. https://doi.org/10.1109/TBME.2009.2039643

Dumpuri, P., Thompson, R. C., Dawant, B. M., Cao, A., & Miga, M. I. (2007). An atlas-based method to compensate for brain shift: preliminary results. *Med Image Anal*, *11*(2), 128-145. https://doi.org/10.1016/j.media.2006.11.002

Elias, W. J., Fu, K. M., & Frysinger, R. C. (2007). Cortical and subcortical brain shift during stereotactic procedures. *J Neurosurg*, *107*(5), 983-988. https://doi.org/10.3171/JNS-07/11/0983

Enchev, Y. (2009). Neuronavigation: geneology, reality, and prospects. *Neurosurgical Focus FOC*,

27(3), E11. https://doi.org/10.3171/2009.6.Focus09109

Fan, X., Roberts, D. W., Olson, J. D., Ji, S., Schaewe, T. J., Simon, D. A., & Paulsen, K. D. (2018). Image Updating for Brain Shift Compensation During Resection. *Oper Neurosurg (Hagerstown)*, *14*(4), 402-411. https://doi.org/10.1093/ons/opx123

Ferrant, M., Nabavi, A., Macq, B., Jolesz, F. A., Kikinis, R., & Warfield, S. K. (2001). Registration of 3-d intraoperative MR images of the brain using a finite-element biomechanical model. *IEEE Transactions on Medical Imaging*, *20*(12), 1384-1397. https://doi.org/10.1109/42.974933

Frey, D., Strack, V., Wiener, E., Jussen, D., Vajkoczy, P., & Picht, T. (2012). A new approach for corticospinal tract reconstruction based on navigated transcranial stimulation and standardized fractional anisotropy values. *Neuroimage*, *62*(3), 1600-1609. https://doi.org/10.1016/j.neuroimage.2012.05.059

Ganslandt, O., Buchfelder, M., Hastreiter, P., Grummich, P., Fahlbusch, R., & Nimsky, C. (2004). Magnetic source imaging supports clinical decision making in glioma patients. *Clin Neurol Neurosurg*, *107*(1), 20-26. https://doi.org/10.1016/j.clineuro.2004.02.027

Ganslandt, O., Fahlbusch, R., Nimsky, C., Kober, H., Moller, M., Steinmeier, R., . . . Vieth, J. (1999). Functional neuronavigation with magnetoencephalography: outcome in 50 patients with lesions around the motor cortex. *Neurosurg Focus*, *6*(3), e3. https://doi.org/10.3171/foc.1999.6.3.6

Gerard, I. J., & Collins, D. L. (2015). An analysis of tracking error in image-guided neurosurgery. *Int J Comput Assist Radiol Surg*, *10*(10), 1579-1588. https://doi.org/10.1007/s11548-014-1145-2

Gerard, I. J., Kersten-Oertel, M., Petrecca, K., Sirhan, D., Hall, J. A., & Collins, D. L. (2017). Brain shift in neuronavigation of brain tumors: A review. *Med Image Anal*, *35*, 403-420. https://doi.org/10.1016/j.media.2016.08.007

Gerhardt, J., Sollmann, N., Hiepe, P., Kirschke, J. S., Meyer, B., Krieg, S. M., & Ringel, F. (2019). Retrospective distortion correction of diffusion tensor imaging data by semi-elastic image fusion - Evaluation by means of anatomical landmarks. *Clin Neurol Neurosurg*, *183*, 105387. https://doi.org/10.1016/j.clineuro.2019.105387

Ginat, D. T., Swearingen, B., Curry, W., Cahill, D., Madsen, J., & Schaefer, P. W. (2014). 3 Tesla intraoperative MRI for brain tumor surgery. *J Magn Reson Imaging*, *39*(6), 1357-1365. https://doi.org/10.1002/jmri.24380

Giordano, M., Nabavi, A., Gerganov, V. M., Javadi, A. S., Samii, M., Fahlbusch, R., & Samii, A. (2015). Assessment of quantitative corticospinal tract diffusion changes in patients affected by subcortical gliomas using common available navigation software. *Clin Neurol Neurosurg*, *136*, 1-4. https://doi.org/10.1016/j.clineuro.2015.05.004

Glasser, M. F., & Rilling, J. K. (2008). DTI tractography of the human brain's language pathways. *Cereb Cortex*, *18*(11), 2471-2482. https://doi.org/10.1093/cercor/bhn011

Hastreiter, P., Rezk-Salama, C., Soza, G., Bauer, M., Greiner, G., Fahlbusch, R., . . . Nimsky, C. (2004). Strategies for brain shift evaluation. *Med Image Anal*, *8*(4), 447-464. https://doi.org/10.1016/j.media.2004.02.001

Hatiboglu, M. A., Weinberg, J. S., Suki, D., Rao, G., Prabhu, S. S., Shah, K., . . . Sawaya, R. (2009). Impact of intraoperative high-field magnetic resonance imaging guidance on glioma surgery: a prospective volumetric analysis. *Neurosurgery*, *64*(6), 1073-1081; discussion 1081. https://doi.org/10.1227/01.NEU.0000345647.58219.07

Heimann, T., van Ginneken, B., Styner, M. A., Arzhaeva, Y., Aurich, V., Bauer, C., . . . Wolf, I. (2009). Comparison and evaluation of methods for liver segmentation from CT datasets. *IEEE Trans Med Imaging*, *28*(8), 1251-1265. https://doi.org/10.1109/TMI.2009.2013851

Hervey-Jumper, S. L., Li, J., Lau, D., Molinaro, A. M., Perry, D. W., Meng, L., & Berger, M. S. (2015). Awake craniotomy to maximize glioma resection: methods and technical nuances over a 27-year period. *J Neurosurg*, *123*(2), 325-339. https://doi.org/10.3171/2014.10.JNS141520

Huang, H., Zhang, J., van Zijl, P. C., & Mori, S. (2004). Analysis of noise effects on DTI-based tractography using the brute-force and multi-ROI approach. *Magn Reson Med*, *52*(3), 559-565. https://doi.org/10.1002/mrm.20147

Ille, S., Engel, L., Albers, L., Schroeder, A., Kelm, A., Meyer, B., & Krieg, S. M. (2019). Functional Reorganization of Cortical Language Function in Glioma Patients—A Preliminary Study [Original Research]. *Frontiers in Oncology*, *9*(446). https://doi.org/10.3389/fonc.2019.00446

Ille, S., Schroeder, A., Wagner, A., Negwer, C., Kreiser, K., Meyer, B., & Krieg, S. M. (2021a). Intraoperative MRI-based elastic fusion for anatomically accurate tractography of the corticospinal tract: correlation with intraoperative neuromonitoring and clinical status. *Neurosurg Focus*, *50*(1), E9. https://doi.org/10.3171/2020.10.FOCUS20774

Ille, S., Schwendner, M., Zhang, W., Schroeder, A., Meyer, B., & Krieg, S. M. (2021b). Tractography

for Subcortical Resection of Gliomas Is Highly Accurate for Motor and Language Function: ioMRI-Based Elastic Fusion Disproves the Severity of Brain Shift. *Cancers (Basel)*, *13*(8). https://doi.org/10.3390/cancers13081787

Imbault, M., Chauvet, D., Gennisson, J. L., Capelle, L., & Tanter, M. (2017). Intraoperative Functional Ultrasound Imaging of Human Brain Activity. *Sci Rep*, *7*(1), 7304. https://doi.org/10.1038/s41598-017-06474-8

Ivanov, M., & Ciurea, A. V. (2009). Neuronavigation. Principles. Surgical technique. *J Med Life*, *2*(1), 29-35. https://www.ncbi.nlm.nih.gov/pubmed/20108488

https://www.ncbi.nlm.nih.gov/pmc/articles/PMC5051478/pdf/JMedLife-02-29.pdf

Javadi, S. A., Nabavi, A., Giordano, M., Faghihzadeh, E., & Samii, A. (2017). Evaluation of Diffusion Tensor Imaging-Based Tractography of the Corticospinal Tract: A Correlative Study With Intraoperative Magnetic Resonance Imaging and Direct Electrical Subcortical Stimulation. *Neurosurgery*, *80*(2), 287-299. https://doi.org/10.1227/NEU.0000000000001347

Kamada, K., Houkin, K., Takeuchi, F., Ishii, N., Ikeda, J., Sawamura, Y., . . . Iwasaki, Y. (2003). Visualization of the eloquent motor system by integration of MEG, functional, and anisotropic diffusion-weighted MRI in functional neuronavigation. *Surg Neurol*, *59*(5), 352-361; discussion 361-352. https://doi.org/10.1016/s0090-3019(03)00018-1

Kelly, P. J., Kall, B. A., Goerss, S., & Earnest, F. t. (1986). Computer-assisted stereotaxic laser resection of intra-axial brain neoplasms. *J Neurosurg*, *64*(3), 427-439. https://doi.org/10.3171/jns.1986.64.3.0427

Khalid, M. T., Allen, J. C., Jr., King, N. K. K., Rao, J. P., Tan, E. T. W., See, A. A. Q., . . . Ng, W. H. (2017). Characterization of Pyramidal Tract Shift in High-Grade Glioma Resection. *World Neurosurg*, *107*, 612-622. https://doi.org/10.1016/j.wneu.2017.08.004

Khan, I., Waqas, M., & Shamim, M. S. (2017). Role of Intra-operative MRI (iMRI) in Improving Extent of Resection and Survival in Patients with Glioblastoma Multiforme. *J Pak Med Assoc*, *67*(7), 1121-1123. https://www.ncbi.nlm.nih.gov/pubmed/28770902

Krieg, S. M., Lioumis, P., Makela, J. P., Wilenius, J., Karhu, J., Hannula, H., . . . Picht, T. (2017). Protocol for motor and language mapping by navigated TMS in patients and healthy volunteers; workshop report. *Acta Neurochir (Wien)*, *159*(7), 1187-1195. https://doi.org/10.1007/s00701-017-3187-z

Krivosheya, D., Rao, G., Tummala, S., Kumar, V., Suki, D., Bastos, D. C. A., & Prabhu, S. S. (2019). Impact of Multi-modality Monitoring Using Direct Electrical Stimulation to Determine Corticospinal Tract Shift and Integrity in Tumors using the Intraoperative MRI. *J Neurol Surg A Cent Eur Neurosurg*. https://doi.org/10.1055/s-0039-1698383

Kubben, P. L., ter Meulen, K. J., Schijns, O. E., ter Laak-Poort, M. P., van Overbeeke, J. J., & van Santbrink, H. (2011). Intraoperative MRI-guided resection of glioblastoma multiforme: a systematic review. *Lancet Oncol*, *12*(11), 1062-1070. https://doi.org/10.1016/S1470-2045(11)70130-9

Kuhnt, D., Bauer, M. H., & Nimsky, C. (2012). Brain shift compensation and neurosurgical image fusion using intraoperative MRI: current status and future challenges. *Crit Rev Biomed Eng*, *40*(3), 175-185. https://doi.org/10.1615/critrevbiomedeng.v40.i3.20

Lacroix, M., Abi-Said, D., Fourney, D. R., Gokaslan, Z. L., Shi, W., DeMonte, F., . . . Sawaya, R. (2001). A multivariate analysis of 416 patients with glioblastoma multiforme: prognosis, extent of resection, and survival. *J Neurosurg*, *95*(2), 190-198. https://doi.org/10.3171/jns.2001.95.2.0190

Leclercq, D., Delmaire, C., de Champfleur, N. M., Chiras, J., & Lehericy, S. (2011). Diffusion tractography: methods, validation and applications in patients with neurosurgical lesions. *Neurosurg Clin N Am*, *22*(2), 253-268, ix. https://doi.org/10.1016/j.nec.2010.11.004

Leclercq, D., Duffau, H., Delmaire, C., Capelle, L., Gatignol, P., Ducros, M., . . . Lehericy, S. (2010). Comparison of diffusion tensor imaging tractography of language tracts and intraoperative subcortical stimulations. *J Neurosurg*, *112*(3), 503-511. https://doi.org/10.3171/2009.8.JNS09558

Li, S., Sun, H., Liu, X., Ren, X., Hao, S., Zeng, M., . . . Han, R. (2020). Mannitol Improves Intraoperative Brain Relaxation in Patients With a Midline Shift Undergoing Supratentorial Tumor Surgery: A Randomized Controlled Trial. *J Neurosurg Anesthesiol*, *32*(4), 307-314. https://doi.org/10.1097/ANA.0000000000000585

Lubrano, V., Draper, L., & Roux, F.-E. (2010). What Makes Surgical Tumor Resection Feasible in Broca's Area? Insights Into Intraoperative Brain Mapping. *Neurosurgery*, *66*(5), 868-875. https://doi.org/10.1227/01.Neu.0000368442.92290.04

Luo, M., Frisken, S. F., Weis, J. A., Clements, L. W., Unadkat, P., Thompson, R. C., . . . Miga, M. I.

(2017). Retrospective study comparing model-based deformation correction to intraoperative magnetic resonance imaging for image-guided neurosurgery. *J Med Imaging (Bellingham)*, *4*(3), 035003. https://doi.org/10.1117/1.JMI.4.3.035003

Maesawa, S., Fujii, M., Nakahara, N., Watanabe, T., Wakabayashi, T., & Yoshida, J. (2010). Intraoperative tractography and motor evoked potential (MEP) monitoring in surgery for gliomas around the corticospinal tract. *World Neurosurg*, *74*(1), 153-161. https://doi.org/10.1016/j.wneu.2010.03.022

Mahboob, S., McPhillips, R., Qiu, Z., Jiang, Y., Meggs, C., Schiavone, G., . . . Eljamel, S. (2016). Intraoperative Ultrasound-Guided Resection of Gliomas: A Meta-Analysis and Review of the Literature. *World Neurosurg*, *92*, 255-263. https://doi.org/10.1016/j.wneu.2016.05.007

Mahvash, M., Boettcher, I., Petridis, A. K., & Besharati Tabrizi, L. (2017). Image guided surgery versus conventional brain tumor and craniotomy localization. *J Neurosurg Sci*, *61*(1), 8-13. https://doi.org/10.23736/S0390-5616.16.03142-8

McAuliffe, N., Nicholson, S., Rigamonti, A., Hare, G. M. T., Cusimano, M., Garavaglia, M., . . . Das, S. (2018). Awake craniotomy using dexmedetomidine and scalp blocks: a retrospective cohort study. *Can J Anaesth*, *65*(10), 1129-1137. https://doi.org/10.1007/s12630-018-1178-z (Craniotomie sur patient eveille utilisant la dexmedetomidine et des blocs des nerfs du scalp: une etude de cohorte retrospective.)

Milian, M., Luerding, R., Ploppa, A., Decker, K., Psaras, T., Tatagiba, M., . . . Feigl, G. C. (2013). "Imagine your neighbor mows the lawn": a pilot study of psychological sequelae due to awake craniotomy: clinical article. *J Neurosurg*, *118*(6), 1288-1295. https://doi.org/10.3171/2013.2.JNS121254

Mori, S., & van Zijl, P. C. (2002). Fiber tracking: principles and strategies - a technical review. *NMR Biomed*, *15*(7-8), 468-480. https://doi.org/10.1002/nbm.781

Morin, F., Courtecuisse, H., Reinertsen, I., Le Lann, F., Palombi, O., Payan, Y., & Chabanas, M. (2017). Brain-shift compensation using intraoperative ultrasound and constraint-based biomechanical simulation. *Med Image Anal*, *40*, 133-153. https://doi.org/10.1016/j.media.2017.06.003

Munnich, T., Klein, J., Hattingen, E., Noack, A., Herrmann, E., Seifert, V., . . . Forster, M. T. (2019). Tractography Verified by Intraoperative Magnetic Resonance Imaging and Subcortical

Stimulation During Tumor Resection Near the Corticospinal Tract. *Oper Neurosurg (Hagerstown)*, *16*(2), 197-210. https://doi.org/10.1093/ons/opy062

Nabavi, A., Black, P. M., Gering, D. T., Westin, C. F., Mehta, V., Pergolizzi, R. S., Jr., . . . Jolesz, F. A. (2001). Serial intraoperative magnetic resonance imaging of brain shift. *Neurosurgery*, *48*(4), 787-797; discussion 797-788. https://doi.org/10.1097/00006123-200104000-00019

Napolitano, M., Vaz, G., Lawson, T. M., Docquier, M. A., van Maanen, A., Duprez, T., & Raftopoulos, C. (2014). Glioblastoma surgery with and without intraoperative MRI at 3.0T. *Neurochirurgie*, *60*(4), 143-150. https://doi.org/10.1016/j.neuchi.2014.03.010

Negwer, C., Hiepe, P., Meyer, B., & Krieg, S. M. (2020). Elastic Fusion Enables Fusion of Intraoperative Magnetic Resonance Imaging Data with Preoperative Neuronavigation Data. *World Neurosurg*, *142*, e223-e228. https://doi.org/10.1016/j.wneu.2020.06.166

Negwer, C., Sollmann, N., Ille, S., Hauck, T., Maurer, S., Kirschke, J. S., . . . Krieg, S. M. (2017). Language pathway tracking: comparing nTMS-based DTI fiber tracking with a cubic ROIs-based protocol. *J Neurosurg*, *126*(3), 1006-1014. https://doi.org/10.3171/2016.2.JNS152382

Nimsky, C. (2011). Intraoperative acquisition of fMRI and DTI. *Neurosurg Clin N Am*, *22*(2), 269-277, ix. https://doi.org/10.1016/j.nec.2010.11.005

Nimsky, C., Ganslandt, O., & Fahlbusch, R. (2007). Implementation of fiber tract navigation. *Neurosurgery*, *61*(1 Suppl), 306-317; discussion 317-308. https://doi.org/10.1227/01.neu.0000279224.83998.7d

Nimsky, C., Ganslandt, O., Hastreiter, P., & Fahlbusch, R. (2001). Intraoperative compensation for brain shift. *Surg Neurol*, *56*(6), 357-364; discussion 364-355. https://doi.org/10.1016/s0090-3019(01)00628-0

Nimsky, C., Ganslandt, O., Hastreiter, P., Wang, R., Benner, T., Sorensen, A. G., & Fahlbusch, R. (2005). Intraoperative diffusion-tensor MR imaging: shifting of white matter tracts during neurosurgical procedures--initial experience. *Radiology*, *234*(1), 218-225. https://doi.org/10.1148/radiol.2341031984

Nimsky, C., Ganslandt, O., Merhof, D., Sorensen, A. G., & Fahlbusch, R. (2006). Intraoperative visualization of the pyramidal tract by diffusion-tensor-imaging-based fiber tracking. *Neuroimage*, *30*(4), 1219-1229. https://doi.org/10.1016/j.neuroimage.2005.11.001

Ostry, S., Belsan, T., Otahal, J., Benes, V., & Netuka, D. (2013). Is intraoperative diffusion tensor imaging at 3.0T comparable to subcortical corticospinal tract mapping? *Neurosurgery*, *73*(5), 797-807; discussion 806-797. https://doi.org/10.1227/NEU.0000000000000087

Ottenhausen, M., Krieg, S. M., Meyer, B., & Ringel, F. (2015). Functional preoperative and intraoperative mapping and monitoring: increasing safety and efficacy in glioma surgery. *Neurosurg Focus*, *38*(1), E3. https://doi.org/10.3171/2014.10.FOCUS14611

Prada, F., Del Bene, M., Mattei, L., Lodigiani, L., DeBeni, S., Kolev, V., . . . DiMeco, F. (2015). Preoperative magnetic resonance and intraoperative ultrasound fusion imaging for real-time neuronavigation in brain tumor surgery. *Ultraschall Med*, *36*(2), 174-186. https://doi.org/10.1055/s-0034-1385347

Riva, M., Hiepe, P., Frommert, M., Divenuto, I., Gay, L. G., Sciortino, T., . . . Bello, L. (2019). Intraoperative Computed Tomography and Finite Element Modelling for Multimodal Image Fusion in Brain Surgery. *Oper Neurosurg (Hagerstown)*. https://doi.org/10.1093/ons/opz196

Roberts, D. W., Strohbehn, J. W., Hatch, J. F., Murray, W., & Kettenberger, H. (1986). A frameless stereotaxic integration of computerized tomographic imaging and the operating microscope. *J Neurosurg*, *65*(4), 545-549. https://doi.org/10.3171/jns.1986.65.4.0545

Roca, E., Pallud, J., Guerrini, F., Panciani, P. P., Fontanella, M., & Spena, G. (2019). Stimulation-related intraoperative seizures during awake surgery: a review of available evidences. *Neurosurg Rev*. https://doi.org/10.1007/s10143-019-01214-0

Romano, A., D'Andrea, G., Calabria, L. F., Coppola, V., Espagnet, C. R., Pierallini, A., . . . Bozzao, A. (2011). Pre- and intraoperative tractographic evaluation of corticospinal tract shift. *Neurosurgery*, *69*(3), 696-704; discussion 704-695. https://doi.org/10.1227/NEU.0b013e31821a8555

Rosenstock, T., Giampiccolo, D., Schneider, H., Runge, S. J., Bahrend, I., Vajkoczy, P., & Picht, T. (2017). Specific DTI seeding and diffusivity-analysis improve the quality and prognostic value of TMS-based deterministic DTI of the pyramidal tract. *Neuroimage Clin*, *16*, 276-285. https://doi.org/10.1016/j.nicl.2017.08.010

Roux, F. E., Ranjeva, J. P., Boulanouar, K., Manelfe, C., Sabatier, J., Tremoulet, M., & Berry, I. (1997). Motor functional MRI for presurgical evaluation of cerebral tumors. *Stereotact Funct Neurosurg*, *68*(1-4 Pt 1), 106-111. https://doi.org/10.1159/000099910

Sabbah, P., Leveque, C., Dutertre, G., Nioche, C., Bellegou, N., Pouit, B., . . . Cordoliani, Y. S. (2000). [Clinical application of functional MRI: a strategic tool for neurosurgery]. *J Neuroradiol*, *27*(4), 226-232. https://www.ncbi.nlm.nih.gov/pubmed/11223613 (Application clinique de l'IRM fonctionnelle: aide a la strategie neurochirurgicale.)

Schichor, C., Terpolilli, N., Thorsteinsdottir, J., & Tonn, J. C. (2017). Intraoperative Computed Tomography in Cranial Neurosurgery. *Neurosurg Clin N Am*, *28*(4), 595-602. https://doi.org/10.1016/j.nec.2017.05.010

Schieber, M. H. (2007). Chapter 2 Comparative anatomy and physiology of the corticospinal system. *Handb Clin Neurol*, *82*, 15-37. https://doi.org/10.1016/S0072-9752(07)80005-4

Schiffbauer, H., Ferrari, P., Rowley, H. A., Berger, M. S., & Roberts, T. P. (2001). Functional activity within brain tumors: a magnetic source imaging study. *Neurosurgery*, *49*(6), 1313-1320; discussion 1320-1311. https://doi.org/10.1097/00006123-200112000-00005

Shah, A. S., Sylvester, P. T., Yahanda, A. T., Vellimana, A. K., Dunn, G. P., Evans, J., . . . Chicoine, M. R. (2020). Intraoperative MRI for newly diagnosed supratentorial glioblastoma: a multicenter-registry comparative study to conventional surgery. *J Neurosurg*, 1-10. https://doi.org/10.3171/2020.6.JNS19287

Sinha, T. K., Dawant, B. M., Duay, V., Cash, D. M., Weil, R. J., Thompson, R. C., . . . Miga, M. I. (2005). A method to track cortical surface deformations using a laser range scanner. *IEEE Transactions on Medical Imaging*, *24*(6), 767-781. https://doi.org/10.1109/TMI.2005.848373

Skrinjar, O., Nabavi, A., & Duncan, J. (2002). Model-driven brain shift compensation. *Med Image Anal*, *6*(4), 361-373. https://doi.org/10.1016/s1361-8415(02)00062-2

Sollmann, N., Kelm, A., Ille, S., Schroder, A., Zimmer, C., Ringel, F., . . . Krieg, S. M. (2018a). Setup presentation and clinical outcome analysis of treating highly language-eloquent gliomas via preoperative navigated transcranial magnetic stimulation and tractography. *Neurosurg Focus*, *44*(6), E2. https://doi.org/10.3171/2018.3.FOCUS1838

Sollmann, N., Krieg, S. M., Saisanen, L., & Julkunen, P. (2021). Mapping of Motor Function with Neuronavigated Transcranial Magnetic Stimulation: A Review on Clinical Application in Brain Tumors and Methods for Ensuring Feasible Accuracy. *Brain Sci*, *11*(7). https://doi.org/10.3390/brainsci11070897

Sollmann, N., Negwer, C., Ille, S., Maurer, S., Hauck, T., Kirschke, J. S., . . . Krieg, S. M. (2016).

Feasibility of nTMS-based DTI fiber tracking of language pathways in neurosurgical patients using a fractional anisotropy threshold. *J Neurosci Methods*, *267*, 45-54. https://doi.org/10.1016/j.jneumeth.2016.04.002

Sollmann, N., Wildschuetz, N., Kelm, A., Conway, N., Moser, T., Bulubas, L., . . . Krieg, S. M. (2018b). Associations between clinical outcome and navigated transcranial magnetic stimulation characteristics in patients with motor-eloquent brain lesions: a combined navigated transcranial magnetic stimulation-diffusion tensor imaging fiber tracking approach. *J Neurosurg*, *128*(3), 800-810. https://doi.org/10.3171/2016.11.JNS162322

Stark, A. M., van de Bergh, J., Hedderich, J., Mehdorn, H. M., & Nabavi, A. (2012). Glioblastoma: clinical characteristics, prognostic factors and survival in 492 patients. *Clin Neurol Neurosurg*, *114*(7), 840-845. https://doi.org/10.1016/j.clineuro.2012.01.026

Stieglitz, L. H., Fichtner, J., Andres, R., Schucht, P., Krähenbühl, A.-K., Raabe, A., & Beck, J. (2013). The Silent Loss of Neuronavigation Accuracy: A Systematic Retrospective Analysis of Factors Influencing the Mismatch of Frameless Stereotactic Systems in Cranial Neurosurgery. *Neurosurgery*, *72*(5), 796-807. https://doi.org/10.1227/NEU.0b013e318287072d

Stufflebeam, S. M. (2011). Clinical magnetoencephalography for neurosurgery. *Neurosurg Clin N Am*, *22*(2), 153-167, vii-viii. https://doi.org/10.1016/j.nec.2010.11.006

Taha, A. A., & Hanbury, A. (2015). Metrics for evaluating 3D medical image segmentation: analysis, selection, and tool. *BMC Med Imaging*, *15*, 29. https://doi.org/10.1186/s12880-015-0068-x

Taylor, P. A., Alhamud, A., van der Kouwe, A., Saleh, M. G., Laughton, B., & Meintjes, E. (2016). Assessing the performance of different DTI motion correction strategies in the presence of EPI distortion correction. *Hum Brain Mapp*, *37*(12), 4405-4424. https://doi.org/10.1002/hbm.23318

Tharin, S., & Golby, A. (2007). Functional brain mapping and its applications to neurosurgery. *Neurosurgery*, *60*(4 Suppl 2), 185-201; discussion 201-182. https://doi.org/10.1227/01.NEU.0000255386.95464.52

Thomas, N. W. D., & Sinclair, J. (2015). Image-Guided Neurosurgery: History and Current Clinical Applications. *J Med Imaging Radiat Sci*, *46*(3), 331-342. https://doi.org/10.1016/j.jmir.2015.06.003

Vargas, M. I., Delavelle, J., Kohler, R., Becker, C. D., & Lovblad, K. (2009). Brain and spine MRI

artifacts at 3Tesla. *J Neuroradiol*, *36*(2), 74-81. https://doi.org/10.1016/j.neurad.2008.08.001

Wadley, J., Dorward, N., Kitchen, N., & Thomas, D. (1999a). Pre-operative planning and intra-operative guidance in modern neurosurgery: a review of 300 cases. *Ann R Coll Surg Engl*, *81*(4), 217-225. https://www.ncbi.nlm.nih.gov/pubmed/10615186 https://www.ncbi.nlm.nih.gov/pmc/articles/PMC2503267/pdf/annrcse01620-0009.pdf

Wadley, J., Kitchen, N., & Thomas, D. (1999b). Image-guided neurosurgery. *Hosp Med*, *60*(1), 34-38. https://doi.org/10.12968/hosp.1999.60.1.1022

Wang, M. N., & Song, Z. J. (2011). Classification and analysis of the errors in neuronavigation. *Neurosurgery*, *68*(4), 1131-1143; discussion 1143. https://doi.org/10.1227/NEU.0b013e318209cc45

Weiss, C., Tursunova, I., Neuschmelting, V., Lockau, H., Nettekoven, C., Oros-Peusquens, A. M., . . . Grefkes, C. (2015). Improved nTMS- and DTI-derived CST tractography through anatomical ROI seeding on anterior pontine level compared to internal capsule. *Neuroimage Clin*, *7*, 424-437. https://doi.org/10.1016/j.nicl.2015.01.006

Yokoyama, Y., Yamada, Y., Kosugi, K., Yamada, M., Narita, K., Nakahara, T., . . . Jinzaki, M. (2021). Effect of gravity on brain structure as indicated on upright computed tomography. *Sci Rep*, *11*(1), 392. https://doi.org/10.1038/s41598-020-79695-z

Young, R. M., Jamshidi, A., Davis, G., & Sherman, J. H. (2015). Current trends in the surgical management and treatment of adult glioblastoma. *Ann Transl Med*, *3*(9), 121. https://doi.org/10.3978/j.issn.2305-5839.2015.05.10

Yu, Y., Bourantas, G., Zwick, B., Joldes, G., Kapur, T., Frisken, S., . . . Miller, K. (2022). Computer simulation of tumour resection-induced brain deformation by a meshless approach. *Int J Numer Method Biomed Eng*, *38*(1), e3539. https://doi.org/10.1002/cnm.3539

Zhang, W., Ille, S., Schwendner, M., Wiestler, B., Meyer, B., & Krieg, S. M. (2022). Tracking motor and language eloquent white matter pathways with intraoperative fiber tracking versus preoperative tractography adjusted by intraoperative MRI-based elastic fusion. *J Neurosurg*, 1-10. https://doi.org/10.3171/2021.12.JNS212106

Zhuang, D. X., Liu, Y. X., Wu, J. S., Yao, C. J., Mao, Y., Zhang, C. X., . . . Zhou, L. F. (2011). A sparse intraoperative data-driven biomechanical model to compensate for brain shift during neuronavigation. *AJNR Am J Neuroradiol*, *32*(2), 395-402. https://doi.org/10.3174/ajnr.A2288

Zou, K. H., Warfield, S. K., Bharatha, A., Tempany, C. M., Kaus, M. R., Haker, S. J., . . . Kikinis, R. (2004). Statistical validation of image segmentation quality based on a spatial overlap index. *Acad Radiol*, *11*(2), 178-189. https://doi.org/10.1016/s1076-6332(03)00671-8

9. LIST OF FIGURES

10. LIST OF TABLES

11. ACKNOWLEDGEMENT

I would like to express my sincere and deepest gratitude to my supervisor, Prof. Dr. med. Sandro Krieg, for offering me the opportunity to be a doctoral candidate and continuous supporting me with enormous motivations, encouragements, and inspirational ideas during my research. It was a great privilege and honor to work and study under his guidance. His rigorous attitude towards work and scientific research always inspires me.

I also must express my great appreciation to my mentor, Priv.-Doz. Dr. med. Sebastian Ille, who took time to advise me for my research projects. I could not complete my projects or finish this thesis without his instructive comments and valuable suggestions. Thanks for his understanding, tolerance and constant support during my research period.

I would also like to thank Mr. Axel Schröder. I still remember the warm and friendly welcome when I first step into the office. Thanks to him for his instruction and training in the operation of software and nTMS instrument. My special thanks go to Dr.-Ing. Patrick Hiepe for his giant help and technical support. Many thanks to Dr. Ann-Katrin Ohlerth for her careful correction of my thesis in front of grammar, as well as precious suggestions in contents. I would like to express my appreciation to Dr. med. Maximilian Schwendner for his revision and advice of project-related publication. Many thanks to all my friends and colleagues, including Dr. med. Haosu Zhang, Marc Grziwotz, Severin Schramm, Franziska Hausler, Yangyang Jiang, Corinna Börner, Leonie Kram, Beate Neu, Enrike Rosenkranz, Verena Schäferin, Dr. med. Raimunde Liang and Zhenyu Gong. I value our friendships very much.

Most importantly, none of this could have happened without my family. I must express my very profound appreciation to my wife, Jin, for her accompanying me to study and live together in Germany, and for her constant and tender encouragement during my doctoral study. She will always be my cherished love. I must also thank to my parents and my parents-in-law for their continued unconditional supports.

Last, I acknowledge the financial support from the China Scholarship Council which provides funding for my doctoral study in Germany.